SIAM J. SCI. STAT. COMPUT.
Vol. 10, No. 2, pp. 298-327, March 1989

005

A STUDY OF THE VORTEX SHEET METHOD AND ITS RATE OF CONVERGENCE*

ELBRIDGE GERRY PUCKETT†

Abstract. The subject of this study is Chorin's vortex sheet method, which is used to solve the Prandtl boundary layer equations and to impose the no-slip boundary condition in the random vortex method solution of the Navier-Stokes equations. This is a particle method in which the particles carry concentrations of vorticity and undergo a random walk to approximate the diffusion of vorticity in the boundary layer. During the random walk, particles are created at the boundary in order to satisfy the no-slip boundary condition. It is proved that in each of the L^1, L^2, and L^∞ norms the random walk and particle creation, taken together, provide a consistent approximation to the heat equation, subject to the no-slip boundary condition. Furthermore, it is shown that the truncation error is entirely due to the failure to satisfy the no-slip boundary condition exactly. It is demonstrated numerically that the method converges when it is used to model Blasius flow, and rates of convergence are established in terms of the computational parameters. The numerical study reveals that errors grow when the sheet length tends to zero much faster than the maximum sheet strength. The effectiveness of second-order time discretization, sheet tagging, and an alternative particle-creation algorithm are also examined.

Key words. boundary layer equations, particle method, random vortex method, random walk, vorticity

AMS(MOS) subject classifications. 35, 60, 65, 76

1. Introduction.

The vortex sheet method is a numerical method for approximating solutions of the Prandtl boundary layer equations. It was developed by Chorin [9] for use with the random vortex method [8] when approximating solutions of the Navier-Stokes equations in domains with solid boundaries. The vortex sheet method is used in regions adjacent to the boundary, while the random vortex method is used in the interior of the flow. Both methods are particle methods. The particles carry concentrations of vorticity; hence, the velocity field is determined by the particle positions. The particles are advected in this velocity field and then undergo a random walk to model the effects of diffusion. In the vortex sheet method, particles are created on the boundary during the random walk in order to approximately satisfy the no-slip boundary condition. The two methods are coupled by requiring that the circulation around a particle remain the same when it passes from one region to the other and that the velocity imposed on the boundary by the random vortex method is the velocity at infinity in the Prandtl equations. Hybrid vortex sheet/random vortex methods have been successfully used to model such problems as flow past a circular cylinder [5], [6], [36]; driven cavity flow [7], [27]; boundary layer instability [11]; flow past a backward-facing step [32]; turbulent combustion [15], [33], [34]; and wind flow over a building [35].

Much theoretical work has been devoted to understanding the accuracy of the vortex method (i.e., the random vortex method without the random walk used to solve

* Received by the editors June 8, 1987; accepted for publication (in revised form) May 25, 1988. This work was part of the author's Ph.D. dissertation in the Mathematics Department, University of California, Berkeley, California. Portions of this work were performed under the auspices of the Office of Naval Research under contract N00014-76-C-0316 and the U.S. Department of Energy at the Lawrence Berkeley Laboratory under contract DE-AC03-76SF00098 and the Lawrence Livermore National Laboratory under contract W-7405-ENG-48. Portions of this work have appeared, in preliminary form, in *Proc. Seventh GAMM Conference on Numerical Methods in Fluid Mechanics*, Louvain-la-Neuve, Belgium 1987 and in *Proc. First National Fluid Dynamics Congress*, Cincinnati, OH, 1988.

† Lawrence Livermore National Laboratory, Livermore, California 94550.

Euler's equations) [1]–[3], [13], [17]–[19]. Although there are fewer theoretical results for the random vortex method, it has been shown that the method converges in a two-dimensional domain with a free-space boundary condition [16], [24]. There is also a numerical study of the random vortex method [28] and a detailed numerical investigation of a hybrid vortex sheet/random vortex method applied to flow past a rearward-facing step [32]. However, to date there has been no theoretical or numerical work to investigate the effectiveness of the vortex sheet method in approximating solutions of the Prandtl equations. This is the goal of the present work.

We begin by reviewing the Prandtl equations. Then in § 2 we describe the method and discuss two conditions, based on a priori estimates, that the computational parameters must satisfy. In § 3 we show that the sheet-creation algorithm is equivalent to interpolating the tangential velocity on the wall induced by the current positions of the sheets. In § 4 we examine the error after one timestep of the random walk and sheet-creation process. We prove that this process is a consistent approximation to the exact solution of the diffusion equation with the no-slip boundary condition in the sense that the expected value of the computed solution is the exact solution plus some error which goes to zero as the method is refined. We estimate the consistency error in the L^1, L^2, and L^∞ norms and show that this error is entirely due to our failure to satisfy the no-slip boundary condition exactly. We also derive bounds on the variance of the computed solution and the probability distribution of the error after one timestep of the random walk and sheet-creation process. Finally, in § 5 we present the results of extensive computations using the method to approximate Blasius flow. Our numerical results demonstrate that the computed solution converges to the exact solution, provided the parameters are chosen correctly. We endeavor to develop guidelines for choosing these parameters so that the resulting computation is optimally accurate and efficient. We also examine the merits of using a second-order time-integration scheme, a different sheet-creation algorithm, and a variance-reduction technique known as sheet tagging.

1.1. The Prandtl equations. In two dimensions the Prandtl equations [10], [23], [30], [37] are

$$u_t + uu_x + vu_y = -p_x + \nu u_{yy}, \tag{1.1a}$$

$$u_x + v_y = 0, \tag{1.1b}$$

with boundary conditions

$$u(x, 0, t) = 0, \tag{1.1c}$$

$$v(x, 0, t) = 0, \tag{1.1d}$$

$$\lim_{y\to\infty} u(x, y, t) = U(x, t), \tag{1.1e}$$

where x, y are orthogonal coordinates, u is the velocity component in the x direction, v is the component in the y direction, p is the pressure, ν is the kinematic viscosity, and $U(x, t)$ is the free-stream velocity. The free-stream velocity or "velocity at infinity" is independent of y and assumed to be known. We also assume the flow has constant density $\rho = 1$.

These equations are derived from the Navier–Stokes equations under the assumption that the velocity component perpendicular to the boundary is small relative to the tangential component. They are valid for general laminar flows along curved walls, as long as the boundary layer thickness is small compared to the wall's radius of curvature (White [37, p. 256]). Both the boundary layer equations [30] and the vortex

sheet method [11] may be generalized to three dimensions. For simplicity we work in two dimensions and assume that the boundary is a flat wall of length L, beginning at $(0, 0)$ and extending to $(L, 0)$.

It follows from $p_y = 0$ [30, p. 121] that the pressure is imposed on the flow from outside the boundary layer and hence, is a known quantity. Furthermore, by (1.1b) and (1.1d),

$$v(x, y) = -\int_0^y u_x(x, y')\, dy', \tag{1.2}$$

and we see that equations (1.1a)-(1.1e) are in fact an evolution equation for one unknown u.

It will be useful to consider the Prandtl equations in vorticity formulation:

$$\frac{D\omega}{Dt} = \nu\omega_{yy}, \tag{1.3a}$$

$$\omega = -u_y, \tag{1.3b}$$

$$u_x + v_y = 0, \tag{1.3c}$$

where ω is the vorticity, $D/Dt = \partial_t + u\partial_x + v\partial_y$ is the material derivative, and the boundary conditions remain (1.1c)-(1.1e). By (1.3b) and (1.1e),

$$u(x, y, t) = U(x, t) + \int_y^\infty \omega(x, y', t)\, dy', \tag{1.4}$$

and it follows that all unknown quantities may be recovered from the vorticity. Thus, the Prandtl equations may also be viewed as an evolution equation for the vorticity ω. This evolution is governed by equation (1.3a). In the vortex sheet method we split this equation into two parts:

$$\frac{D\omega}{Dt} = 0, \tag{1.5}$$

$$\omega_t = \nu\omega_{yy}, \tag{1.6}$$

and solve each part separately.

2. The vortex sheet method. The vortex sheet method is a fractional step method in which one step consists of solving (1.5) and the other of solving (1.6) subject to the boundary condition (1.1c). The particles, called "sheets," carry piecewise linear concentrations of vorticity and the velocity field is reconstructed from the particle positions using (1.4). (We use the words "sheets" and "particles" interchangeably.) The solution of (1.5) is obtained by passively advecting the sheets in this velocity field. The solution of (1.6) is obtained by creating sheets at the wall in order to (approximately) satisfy (1.1c) and then giving all sheets a random displacement in the y direction, reflecting those which go below the wall. This creation of sheets mimics the physical creation of vorticity at the wall.

2.1. Notation. Let $P_{\Delta t}u^0$ denote the solution at time Δt of the Prandtl equations (1.1a)-(1.1e) with initial data u^0. Similarly, let $A_{\Delta t}u^0$ denote the solution at time Δt of the inviscid equation

$$\frac{Du}{Dt} = -p_x, \tag{2.1a}$$

(2.1b) $$u_x + v_y = 0,$$

(2.1c) $$u(x, \infty, t) = U(x), \qquad t > 0,$$

(2.1d) $$v(x, 0, t) = 0, \qquad t > 0,$$

with initial data u^0, and let $D_{\Delta t}u^0$ denote the solution of the diffusion equation

(2.2a) $$u_t = \nu u_{yy}$$

(2.2b) $$u(x, 0, t) = 0, \qquad t > 0$$

with initial data u^0. (Here and in what follows we suppress explicit mention of the dependence of the free-steam velocity U on the time t for notational convenience.) The vortex sheet method consists of finding approximations $\tilde{A}_{\Delta t}$, $\tilde{D}_{\Delta t}$ to $A_{\Delta t}$, $D_{\Delta t}$ and then approximating $P_{\Delta t}u^0$ with $\tilde{D}_{\Delta t}\tilde{A}_{\Delta t}u^0$. We write $u^k = (P_{\Delta t})^k u^0$ and $\tilde{u}^k = (\tilde{D}_{\Delta t}\tilde{A}_{\Delta t})^k u^0$. We always use the tilde to denote an approximation. Thus, $\tilde{u}^k$ is an approximation to u^k, $\tilde{\omega}^k$ is an approximation to ω^k, etc.

2.2. The approximate velocity field $\tilde{u}^k$. For now we omit all reference to time and consider the vortex sheet method approximation to the velocity field at a fixed instant in time. The principle common to all vortex methods is that the velocity field is completely determined by the vorticity field and boundary conditions. In the vortex sheet method we replace the integral on the right-hand side of (1.4) by the sum

(2.3) $$\tilde{u}(x, y) = U(x) + \sum_j \omega_j b_h(x - x_j) H(y_j - y),$$

where $H(y)$ is the Heaviside function,

$$H(y) = \begin{cases} 0, & x < 0, \\ 1, & x \geqq 0. \end{cases}$$

The function b_h, called the *cutoff* or *smoothing* function, is defined by $b_h(x) = b(x/h)$, where b can be chosen in many ways. All cutoffs that we consider will be normalized so that $b(0) = 1$ and have compact support,

(2.4) $$b(x) = 0 \quad \text{for } |x| \geqq R.$$

Typically, $R = 1$ or $R = 2$. We discuss cutoffs at length in § 3.

Each term of the sum in (2.3) is referred to as a *vortex sheet.* The jth sheet has center (x_j, y_j), *strength* or *weight* ω_j, and length $2Rh$, where R depends on the particular smoothing function chosen. The parameter h is frequently referred to as the "sheet length," even though the actual length is usually nh for some integer $n > 1$. From (2.3) we see that the jump in $\tilde{u}$ along the jth sheet is $\omega_j b_h(x - x_j)$. This is the motivation for referring to the computational elements as "vortex sheets."

We can rewrite (2.3) as

$$\tilde{u}(x, y) = U(x) + \int_y^\infty \sum_j \omega_j b_h(x - x_j)\delta(y_j - y')\, dy'$$

where δ is the Dirac delta function. Thus, our approximation to the vorticity is

$$\tilde{\omega}(x, y) = \sum_j \omega_j b_h(x - x_j)\delta(y_j - y)$$

and we see that each sheet carries a linear concentration of vorticity that varies like $b_h(x - x_j)$ as we move along the line segment $(-Rh \leqq x - x_j \leqq Rh,\ y = y_j)$.

Using (1.2) we find that our approximation to v is given by

$$\tilde{v}(x, y) = -U_x(x)y - \sum \omega_j \partial_x b_h(x - x_j) \min(y, y_j).$$

For cutoffs that are not differentiable everywhere (this is the case for the most commonly used cutoff) we can use a divided difference approximation to $\partial_x b_h$:

$$\tilde{v}(x, y) = -U_x(x)y - \sum \omega_j h^{-1}\left[b_h\left(x + \frac{h}{2} - x_j\right) - b_h\left(x - \frac{h}{2} - x_j\right)\right] \min(y, y_j). \tag{2.5}$$

2.3. Integration of the equations in time. Our approximation $(\tilde{u}, \tilde{v})$ to the velocity field (u, v) is completely determined by the positions of the particles (x_j, y_j) and their weights ω_j. Denote the timestep by Δt, the position of the jth particle at time $k\Delta t$ by (x_j^k, y_j^k) and the velocity field derived from these positions by $(\tilde{u}^k, \tilde{v}^k)$. Given $(\tilde{u}^k, \tilde{v}^k)$ the velocity field at the next timestep is determined as follows.

2.3.1. The advection step. The solution of the advection equation (2.1a)-(2.1d) with initial data $(\tilde{u}^k, \tilde{v}^k)$ is found by moving the sheets according to

$$x_j^{k+1/2} = x_j^k + \Delta t \tilde{u}^k(x_j^k, y_j^k), \tag{2.6a}$$

$$y_j^{k+1/2} = y_j^k + \Delta t \tilde{v}^k(x_j^k, y_j^k). \tag{2.6b}$$

Thus, the velocity field after the first of the two fractional steps, denoted by $(\tilde{u}^{k+1/2}, \tilde{v}^{k+1/2})$, is

$$\tilde{u}^{k+1/2}(x, y) = U(x) + \sum_j \omega_j b_h(x - x_j^{k+1/2}) H(y_j^{k+1/2} - y),$$

$$\tilde{v}^{k+1/2}(x, y) = -U_x(x)y - \sum_j \omega_j \partial_x b_h(x - x_j^{k+1/2}) \min(y, y_j^{k+1/2}).$$

Note that since the sheet strengths remain constant in the advection step, $\tilde{\omega}^{k+1/2} \equiv -\partial_y \tilde{u}^{k+1/2}$ approximates the solution of (1.5) with initial data $\tilde{\omega}^k$ in the sense that vorticity is constant on approximate particle paths $(x_j^k, y_j^k) \to (x_j^{k+1/2}, y_j^{k+1/2})$.

In (2.6a), (2.6b) we have used Euler's method to solve the system of ordinary differential equations (ODEs):

$$\frac{dx_j}{dt} = u(x_j, y_j, t), \tag{2.7a}$$

$$\frac{dy_j}{dt} = v(x_j, y_j, t), \tag{2.7b}$$

with the right-hand side replaced by $\tilde{u}^k$ and $\tilde{v}^k$. We can choose to solve the system (2.7a), (2.7b) with a higher-order ODE solver. Extensive theoretical work (e.g., [1], [21]) has demonstrated the effectiveness of using a higher-order ODE solver in the vortex method solution of the Euler equations. However, to date there has been no such work on the use of a higher-order solution of (2.7a), (2.7b) for the vortex sheet method. In § 5.4 we present the results of a numerical experiment, comparing a second-order solution of (2.7a), (2.7b) with the first-order solution given by (2.6a), (2.6b).

2.3.2. The particle-creation and diffusion step. The second part of the splitting procedure is the random walk solution of (2.2a), (2.2b) with initial data $\tilde{u}^{k+1/2}$. This consists of creating sheets at gridpoints on the wall to approximately satisfy the no-slip boundary condition (1.1c), and then letting all sheets undergo a random walk in the y direction, reflecting those sheets that go below the wall.

Choose h so that the wall length L is an integral multiple of h, $L = rh$. Choose equally spaced points $a_1, \cdots, a_r$ on the wall with $a_1 = h/2$, $a_i - a_{i-1} = h$, and $a_r = L - h/2$. We approximately satisfy (1.1c) by requiring that at the end of every timestep, $\tilde{u}^{k+1}(a_i, 0) \approx 0$. This is accomplished as follows. Let $\omega_{\max}$ denote a computational parameter called the *maximum sheet strength.* All ω_j will be chosen so that $|\omega_j| \leqq \omega_{\max}$.

This is the parameter that most directly influences the accuracy of the random walk. Let $u_i = \tilde{u}^{k+1/2}(a_i, 0)$. At each a_i we create $q_i \geqq 0$ sheets with centers $(x_i, y_i) = (a_i, 0)$ and strengths ω_{il} so that

$$\left| \tilde{u}^{k+1/2}(a_j, 0) + \sum_{i=1}^{r} \sum_{l=1}^{q_i} \omega_{il} b_h(a_j - x_i) H(y_i - 0) \right| = \left| u_j + \sum_{i=1}^{r} \sum_{l=1}^{q_i} \omega_{il} b_h(a_j - a_i) \right| \leqq \omega_{\max}$$

for each j. We assume that for a given i the ω_{il} are all equal and sometimes write ω_i rather than ω_{il}.

We have considerable leeway when choosing q_i and ω_i. We therefore discuss this aspect of the algorithm in greater detail. We begin by describing the version originally proposed by Chorin in [9]. We then present a variation on his idea which leads to fewer sheets at the expense of approximating the no-slip boundary condition less accurately. Assume that $R = 1$ in (2.4). Hence, $b_h(a_i - a_j) = \delta_{ij}$, where δ_{ij} is the Kronecker delta function. This is the case for the most commonly used cutoff. In § 3.3 we will remove this assumption and describe a different creation algorithm for which $R = 2$.

PARTICLE-CREATION ALGORITHM A. In this version a sheet is created at a_i if $|u_i| \geqq \varepsilon$ where, for example, ε might be chosen to be on the order of the computer's roundoff error. Let $[x]$ denote the greatest integer less than or equal to x. If $|u_i| \geqq \varepsilon$, then we create

$$q_i = \begin{cases} |u_i|/\omega_{\max} & \text{if } \omega_{\max} \text{ divides } u_i \text{ evenly,} \\ [|u_i|/\omega_{\max} + 1] & \text{otherwise,} \end{cases}$$

sheets at $(a_i, 0)$, each of strength $\omega_i = -u_i/q_i$. Otherwise we set $q_i = 0$ and create no new sheets at $(a_i, 0)$. As we shall see presently, the random walk does not alter the tangential velocity at the wall. Hence, the tangential velocity at time $(k+1)\Delta t$ satisfies

$$|\tilde{u}^{k+1}(a_i, 0)| = |u_i + q_i \omega_i| < \begin{cases} 0, & \text{if } q_i > 0, \\ \varepsilon, & \text{if } q_i = 0. \end{cases} \tag{2.8}$$

PARTICLE-CREATION ALGORITHM B. An alternate version of this particle-creation algorithm was used in [32], as well as in the present work. At the ith gridpoint we create $q_i = [|u_i|/\omega_{\max}]$ sheets, each with strength $\omega_i = -\text{sign}\,(u_i)\omega_{\max}$ and center $(a_i, 0)$. Our approximation to the tangential velocity at time $(k+1)\Delta t$ now satisfies

$$|\tilde{u}^{k+1}(a_i, 0)| = |u_i - q_i \text{ sign } (u_i)\omega_{\max}| < \omega_{\max}. \tag{2.9}$$

Note that Algorithm B is not Algorithm A with $\varepsilon = \omega_{\max}$, since in Algorithm B all sheet strengths have the same magnitude $\omega_{\max}$. In § 5.6 we will show that this diminishes the number of sheets in the flow without adversely affecting the overall accuracy of the method.

Now let every sheet (including those just created) take a random walk in the y direction, reflecting those sheets that go below the wall. The new particle positions are given by

$$x_j^{k+1} = x_j^{k+1/2}, \qquad y_j^{k+1} = |y_j^{k+1/2} + \zeta_j|$$

where ζ_j is a Gaussian-distributed random number with mean 0 and variance $2\nu\Delta t$. The tangential velocity at time $(k+1)\Delta t$ is therefore

$$\begin{aligned} \tilde{u}^{k+1}(x, y) &= U(x) + \sum_{j=1}^{N_k} \omega_j b_h(x - x_j^{k+1/2}) H(|y_j^{k+1/2} + \zeta_j| - y) \\ &\quad + \sum_{i=1}^{r} \sum_{l=1}^{q_i} \omega_i b_h(x - a_i) H(|\zeta_{il}| - y) \\ &= U(x) + \sum_{j=1}^{N_{k+1}} \omega_j b_h(x - x_j^{k+1}) H(y_j^{k+1} - y) \end{aligned} \tag{2.10}$$

where N_k (respectively, N_{k+1}) is the number of sheets in the flow at time $k\Delta t$ (respectively, time $(k+1)\Delta t$). Using the notation introduced in § 2.1 we write $\tilde{u}^{k+1} = \tilde{D}_{\Delta t}\tilde{u}^{k+1/2}$.

It is appropriate to make several remarks here concerning the random walk and sheet-creation algorithm. Let E denote the expected value with respect to the ζ_j and ζ_{il} in (2.10). A consequence of Theorem 4.1 is that for each $x \in [0, L]$,

$$\tilde{u}^{k+1}(x, 0) = 0 \Rightarrow D_{\Delta t}\tilde{u}^{k+1/2}(x, y) = E[\tilde{D}_{\Delta t}\tilde{u}^{k+1/2}(x, y)]. \tag{2.11}$$

We then show that for either of the creation algorithms described above

$$\|D_{\Delta t}\tilde{u}^{k+1/2}(x, y) - E[\tilde{D}_{\Delta t}\tilde{u}^{k+1/2}(x, y)]\|_s = O((h + \omega_{\max})(\nu\Delta t)^{1/2s}) \tag{2.12}$$

for $s = 1, 2, \infty$. Thus, $\tilde{D}_{\Delta t}\tilde{u}^{k+1/2}$ is a consistent approximation to $D_{\Delta t}\tilde{u}^{k+1/2}$ with truncation error $O((h + \omega_{\max})(\nu\Delta t)^{1/2s})$. It follows from (2.11) and (2.12) that this error is entirely due to our failure to satisfy the no-slip boundary condition exactly. In § 3 we will show that the cutoff function determines how well $\tilde{u}^{k+1}(x, 0)$ satisfies the no-slip boundary condition at each point x on the wall.

In the original version of the vortex sheet method, Chorin created twice as many sheets as needed, the total of which was twice that needed to cancel the velocity at the wall [9, p. 423]. He then let these new sheets random walk *without reflection*, throwing away those sheets that went below the wall. (Of course the other sheets underwent a random walk, with reflection, as above.) In a more recent version [11, p. 6], Chorin again created twice as many sheets as needed, but this time he employed a rejection technique to ensure that *exactly half* of these sheets took their random walk in the positive y direction. However, (2.11) and (2.12) show us that these special procedures are unnecessary. It is sufficient to create sheets as in Algorithms A or B above and allow them to undergo a random walk with reflection. These results also demonstrate that the sheet creation and random walk are part of the same process. Together they comprise one step of a two-step fractional-step method, rather than two separate steps of a three-step method. We emphasize that to obtain (2.11) and (2.12) the new sheets must undergo a random walk immediately after being created, without waiting a timestep before diffusing them from the wall.

2.4. The CFL condition. The most well known and perhaps the only universally acknowledged condition on the parameters in the vortex sheet method is the so-called "CFL" condition. For $U_{\max} \equiv \max U(x)$ this condition states that Δt and h must be chosen so that

$$\Delta t U_{\max} \leqq h. \tag{2.13}$$

This requirement was originally proposed by Chorin in [9]. The justification usually given for (2.13) is that we want to ensure that the distance a sheet travels downstream in one timestep is no more than one sheet length. Hence, sheets created at the ith gridpoint must influence the $(i+1)$st gridpoint before moving on downstream. This is essentially an accuracy criterion (as opposed to a stability criterion). It ensures that information propagating in the streamwise direction influences all features of the flow that are at least $O(h)$.

We now offer another justification for (2.13) which takes into account the rate at which vorticity diffuses across the boundary layer in the vortex sheet method. Consider sheets created at the ith gridpoint a_i at a given timestep. Since the velocity is 0 at the wall, the only movement imparted to these sheets at the next timestep will be due to

the random walk. We seek a condition to ensure that these sheets remain in the boundary layer after this random walk. For the flat plate problem, the boundary layer thickness above a point x is

$$\delta_x \approx 5\sqrt{\frac{\nu x}{U(x)}}$$

(Schlichting [30, p. 140]). The random walks are drawn from a Gaussian distribution with mean 0 and standard deviation $\sigma = \sqrt{2\nu\Delta t}$. Thus, if (2.13) holds, then

$$\frac{5}{2}\sigma \leqq 5\sqrt{\frac{\nu h}{2U(x)}} = \delta_{a_1},$$

where $a_1 = h/2$ is the first gridpoint on the wall. This implies that, on the average, more than 98 percent of the sheets created at a_1 will remain in the boundary layer after taking one timestep. Since the boundary layer increases with increasing x for the flat plate problem, this will also be true for the sheets created at the other gridpoints. Similar conditions may be found for other flows; all that is required is an estimate of the boundary layer thickness.

We now propose another constraint which relates $\omega_{\max}$ to h and Δt. Consider the flat plate problem with initial condition

$$u^0(x, y) = \begin{cases} U_{\max}, & y > 0, \\ 0, & y = 0. \end{cases} \tag{2.14}$$

At the first timestep we need to create K sheets of strength $\omega_{\max}$ at each a_i in order to cancel the velocity $U_{\max}$ just above the wall. Thus, after the random walk, we will have approximated $u(a_i, y)$ by a step function $\tilde{u}(a_i, y)$ with K jumps, each of strength $\omega_{\max}$, such that $\tilde{u}(a_i, 0) = 0$ and $\tilde{u}(a_i, \infty) = U_{\max}$. The task is to choose $\omega_{\max}$ (or equivalently K) in a manner consistent with our choice of Δt and h. It is reasonable to require that we resolve u to the same extent that we are resolving features in the streamwise direction. Therefore, let $K = CL/h$ for some constant C, and let $\omega_{\max} = U_{\max}/K$. Using (2.13) we obtain

$$\omega_{\max} \leqq C_0 \frac{h^2}{\Delta t}, \tag{2.15}$$

where $C_0 = 1/CL$ is a constant with dimensions $1/L$. Our experience with the test problem described in § 5 has been that the best results were obtained with $C_0 < 1/L$. The argument presented here can be easily generalized for flows other than the flat plate problem with initial data (2.14). Since

$$\partial_x \omega_j b_h(x - x_j) = O(\omega_{\max}/h),$$

sheets induce local (nonphysical) streamwise gradients in $\tilde{u}$ and $\tilde{\omega}$ that are $O(\omega_{\max}/h)$. Condition (2.15) relates the size of these gradients to the timestep. In § 5 we present numerical results that demonstrate the importance of (2.15).

2.5. Sheet tagging. In [9] Chorin proposed the following "variance-reduction technique." During the sheet-creation process each sheet is assigned a positive integer, called a *tag*, as follows. Let T_k be the last tag assigned at the kth timestep. Then, during the $(k+1)$st timestep, the first sheet created at every gridpoint is assigned the number $T_k + 1$, the second sheet is assigned $T_k + 2$, and so on until all sheets have a tag. Thus, no two sheets created at the same gridpoint will have the same tag, while one sheet at each gridpoint will have the same tag (except, of course, when more sheets

need to be created at one gridpoint than at another). When the sheets undergo the random walk all sheets with the same tag are assigned the same random walk.

The motivation behind this procedure is twofold. First, if we use the vortex sheet method to model flow past an infinite plate with constant free-stream velocity [10, pp. 92–95], then, with sheet tagging, the vortex sheet method reduces to the random walk solution of the heat equation. This eliminates all error due to the advection step. Second, on heuristic grounds it is believed that vorticity leaving the wall diffuses at the same rate everywhere along the wall, and it was thought that the sheet tagging mimicked this process. Our experience has been that, with the exception of the infinite flat plate problem, sheet tagging does not improve the accuracy of the vortex sheet method. In the remarks after the proof of Theorem 4.7, we show how the variance of the solution can actually *increase* when different sheets with the same tag overlap. In § 5.7 we present the results of numerical experiments that substantiate our contention that the sheet-tagging procedure does not improve the accuracy of the method.

3. Smoothing. It is instructive to examine the smoothing process from the following perspective. Given $\tilde{u}^{k+1/2}$ we would ideally like to create sheets at the wall so that $\tilde{u}^{k+1}$ satisfies (1.1c) for all $x \in [0, L]$. Let $g(x) \equiv \tilde{u}^{k+1/2}(x, 0)$ and let ζ and ζ_j be independent, Gaussian-distributed random variables with mean 0 and variance $2\nu\Delta t$. Then

$$\tilde{u}_{\text{opt}}^{k+1}(x, y) \equiv U(x) + \sum \omega_j b_h(x - x_j^{k+1}) H(|y_j^{k+1/2} + \zeta_j| - y) - g(x) H(|\zeta| - y)$$

is the optimal choice for $\tilde{u}^{k+1}$. For $\tilde{u}_{\text{opt}}^{k+1}$ satisfies the no-slip boundary condition exactly at every x and hence, by (2.11),

$$E[\tilde{u}_{\text{opt}}^{k+1}(x, y)] = D_{\Delta t} \tilde{u}^{k+1/2}(x, y)$$

for all $x \in [0, L]$. However, we need to write $\tilde{u}^{k+1}$ as the sum of vortex sheets. Therefore, our task is to find q_i and ω_{il} such that

$$\tilde{g}(x) \equiv -\sum_{i=1}^{r} \sum_{l=1}^{q_i} \omega_{il} b_h(x - a_i) = \sum_{i=1}^{r} u_i' b_h(x - a_i)$$

is a good approximation to g. This amounts to finding a $\tilde{g}$ that interpolates g at the gridpoints a_i. We will now examine several ways in which this can be done.

3.1. Piecewise constant cutoffs. It is natural to consider choices for the cutoff b that result in piecewise constant $\tilde{g}$. For example, let $b(x) = s(x)$, where s is defined by

$$s(x) = H(\tfrac{1}{2} - |x|). \tag{3.1}$$

It has been observed, however, that the vortex sheet method performs poorly when this cutoff is used. We offer the following possible explanation. For this choice of b the tangential velocity is piecewise constant as a function of x. Consequently, our approximation to the derivative $\partial_x \tilde{u}$ in (2.5) is poor. This in turn leads to large errors in the particle paths through (2.6b).

3.2. Piecewise linear smoothing. An obvious improvement over (3.1) is to choose b so that the resulting $\tilde{g}$ is a piecewise linear approximation to g. Thus, let $b(x) = l(x)$, where

$$l(x) \equiv \begin{cases} 1 - |x| & \text{if } |x| \leqq 1, \\ 0 & \text{otherwise.} \end{cases} \tag{3.2}$$

With this choice of smoothing the functions $b_i(x) \equiv b_h(x - a_i)$, $i = 1, \cdots, r$ are a basis for the space of piecewise linear polynomials on $[0, L]$ with breaks at the a_i (see

Schultz [31, § 2.1]). These functions are frequently referred to as "hat" or "tent" functions. This cutoff was first used by Chorin in [9] and is currently the most widely used cutoff. It has been used successfully for a wide variety of problems. For example, see Cheer [5], [6], Ghoniem, Chorin, and Oppenheim [15], Sethian and Ghoniem [32], Sethian [33], [34], and Tiemroth [36].

3.3. Spline smoothing. Finally, we present an algorithm in which $\tilde{g}$ is a piecewise cubic interpolant of g. This may be accomplished in more than one way. For example, we can choose b so that $\tilde{g}$ is only C^1 at the breakpoints a_i, or C^2 at the a_i, etc. See de Boor [4] or Schultz [31] for details. Here we suggest a cutoff $B(x)$ such that $\tilde{g}$ is C^2 at the breakpoints. Define

$$B(x) \equiv \begin{cases} \frac{1}{4}(2-|x|)^3-(1-|x|)^3, & \text{if } 0 \leqq |x| \leqq 1, \\ \frac{1}{4}(2-|x|)^3, & \text{if } 1 \leqq |x| \leqq 2, \\ 0, & \text{if } |x|>2. \end{cases} \tag{3.3}$$

For $b(x)=B(x)$ the b_h are known as B-splines [4], [31].

Note that with this choice of b the support of b_h is now $4h$, rather than $2h$. Thus, the sheets overlap each other more than with the piecewise linear cutoff defined by (3.2); each sheet centered at a_i now influences three gridpoints, rather than just one. Thus, in the sheet-creation algorithm we can no longer simply choose ω_i so that $|u_i+q_i\omega_i|<\omega_{\max}$. Instead, we must now solve a system of linear equations

$$\tfrac{1}{4}\alpha_{i-1}+\alpha_i+\tfrac{1}{4}\alpha_{i+1}=u_i, \qquad i=2,\cdots,r-1$$

and choose q_i, ω_i so that $|\alpha_i+q_i\omega_i|<\omega_{\max}$. We also must decide what to do at the endpoints, $i=1$ and $i=r$. Endpoint conditions have been extensively studied in the context of the spline interpolation of a function (for example, see de Boor [4]).

For the cubic spline cutoff defined by (3.3) the sheet-creation algorithm should result in fewer sheets. For example, let $L=1$ and consider the periodic problem in which $x=L$ is identified with $x=0$ so we have $a_1=a_{r+1}$, etc. Let $h=0.2$, $\omega_{\max}=3^{-1}$, and $u_i=1.0$, $i=1,\cdots,r$. With the piecewise linear cutoff we will create three sheets at every gridpoint, each of strength $\omega_i=3^{-1}$. On the other hand, with the B-spline cutoff we will create two sheets at every gridpoint, each of strength $\omega_i=3^{-1}$.

Extensive computations with the B-spline cutoff show that, provided (2.15) is satisfied, we do indeed produce fewer sheets. For appropriate choices of the parameters the B-spline cutoff leads to 20–25 percent fewer sheets. However, when the vortex sheet method is used as a stand-alone method for solving the Prandtl equations (as it is in § 5) the added cost of evaluating (3.3) as compared to evaluating (3.2) seems to offset the savings due to fewer sheets. On the other hand, when the vortex sheet method is used in conjunction with the random vortex method, with the sheets eventually becoming vortices, the B-spline cutoff also results in fewer vortices. However, it is not clear whether this will lead to a more economical computation since the B-spline sheets have $\frac{1}{2}$ times more circulation per unit strength than the piecewise linear sheets. The B-spline cutoff does not seem to improve the accuracy of the vortex sheet method or its rate of convergence, most likely because the dominant source of error comes from the use of the random walk to solve (2.2a).

3.4. Smoothing perpendicular to the wall. Let us now consider the smoothness of our approximation as a function of y. From (2.3) it is apparent that $\tilde{u}^k(x, y)$ is a step function in y for each fixed $x \in [0, L]$. This is analogous to the random gradient method described in [25]. In both cases it is natural to inquire what happens if we use something smoother than a step function. In unpublished work, the author replaced the step

function approximation described in § 2 of [25] with a piecewise linear function and used it to compute the traveling wave solution described in § 9.1 of [25]. The piecewise linear version produced a significantly better approximation to the initial data at time $t=0$. After several timesteps, however, the error was comparable to that incurred by the original method. This is because the accuracy in approximating the initial data by a step function is $O(N^{-1})$, where N is the number of particles (jumps in the function). When we use a piecewise linear approximation this accuracy improves. This accounts for the observed decrease in the initial error. However, the error due to solving the diffusion equation by random walking the particles is $O(\sqrt{N}^{-1})$ (see [20], [25], [29], and the results in § 4 below). This rapidly overwhelms the error due to our interpolation of the solution. Similarly, with the vortex sheet method any improvement in accuracy obtained by using a higher-order approximation to $u^k(x, y)$ as a function of y is quickly lost by the random walk.

4. The error due to the random walk operator $\tilde{D}_{\Delta t}$. In this section we prove several bounds on the error that result from using the random walk and sheet-creation algorithm to approximate the exact solution of (2.2a)-(2.2b). The purpose of these estimates is to examine the relationship between the parameters $\nu, \Delta t, \omega_{\max}$, and h and the error made by one timestep of the random walk and sheet-creation process. This analysis also clarifies the relationship between the accuracy with which the no-slip boundary condition is satisfied and the error due to the random walk.

We begin by proving that the random walk and sheet-creation algorithm is consistent in the L^1, L^2, and L^∞ norms:

$$\|E\tilde{D}_{\Delta t}u^0 - D_{\Delta t}u^0\|_s = O((\omega_{\max}+h)(\nu\Delta t)^{1/2s}) \tag{4.1}$$

for $s=1, 2, \infty$. We define u^0, $\tilde{D}_{\Delta t}u^0$ and what we mean by $E\tilde{D}_{\Delta t}u^0$ below. We then derive bounds on the variance of $\tilde{D}_{\Delta t}u^0$ and on the probability distribution of the L^2 error $\|D_{\Delta t}u^0 - \tilde{D}_{\Delta t}u^0\|_2$. These latter bounds are essentially a generalization of Hald's work in [20]. To establish them we first prove

$$\int_0^\infty \operatorname{var} H(|y_j+\zeta_j|-y)\,dy = F(y_j)\sqrt{2\nu\Delta t} \tag{4.2}$$

for some function F, which is bounded between $(2-\sqrt{2})/\sqrt{\pi}$ and $4/\sqrt{\pi}$. (For $y_j=0$ this is Hald's result.) Then, using the fact that the random walks ζ_j taken at a given timestep are independent, we use (4.2) to show

$$\|\operatorname{var}(\tilde{D}_{\Delta t}u^0)\|_1 \leqq C_\nu\sqrt{2\nu\Delta t}\omega_{\max}. \tag{4.3}$$

It follows from (4.1) and (4.3) that the error in the diffusion step decreases as $\nu\to 0$. Thus, we get better results from the random walk at small viscosities for no additional work.

It will be apparent from the proof that (4.3) exhibits the correct dependence on the parameters ν, Δt, and $\omega_{\max}$. In this regard we note that Hald has shown the following:

$$\int_0^\infty \operatorname{var}\Theta(y)\,dy = \frac{(2-\sqrt{2})}{\sqrt{\pi}}\sqrt{2\nu\Delta t}\omega_{\max},$$

where Θ is the random walk solution after one timestep of length Δt to

$$\begin{aligned}
&\Theta_t = \nu\Theta_{yy}, && 0\leqq y<\infty,\\
&\Theta(0, t)=1, && 0<t,\\
&\Theta(y, 0)=0,
\end{aligned}$$

and we have written $\omega_{\max}$ instead of N^{-1} since all of Hald's particles have strength N^{-1}. (This is the second equation in the proof of Theorem 2 in [20].) In other words, the L^1 norm of the variance of Θ is *exactly* $O(\sqrt{\nu \Delta t}\,\omega_{\max})$. In the case of (4.3) equality, in general, fails to hold, but the amount by which the right- and left-hand sides differ does not depend on ν, Δt, or $\omega_{\max}$.

4.1. Notation. In what follows we let u^0 be an arbitrary function of the form

$$u^0(x, y) = U(x) + \sum_{j=1}^{N} \omega_j b_h(x - x_j) H(y_j - y), \tag{4.4}$$

with $|\omega_j| \leqq \omega_{\max}$ for all j. We assume the use of piecewise linear smoothing: $b_h(x) \equiv b(x/h)$ with b defined by (3.2). However, all of the results in this section remain valid with minor modifications if B-spline smoothing is used. We also assume that the y_j in (4.4) have been chosen so that

$$y_i \neq y_j, \qquad i \neq j. \tag{4.5}$$

Therefore, the vorticity field ω^0 corresponding to (4.4) is a measure whose mass is

$$\|\omega^0\| = \int_0^L \int_0^\infty \left| \sum_j \omega_j b_h(x - x_j) \delta(y_j - y) \right| dx\, dy = \sum_j |\omega_j| \int_0^L b_h(x - x_j)\, dx, \tag{4.6}$$

where the sum is over all sheets in the flow. We remark that in the vortex sheet method (without sheet tagging) the probability that $y_i^k = y_j^k$ or $y_i^{k+1/2} = y_j^{k+1/2}$ for some $i \neq j$ is 0. Hence, assumption (4.5) is reasonable.

We assume that the a_i have been chosen as described in § 2.3.2. Let ζ_j and ζ_{il} be independent, Gaussian-distributed random variables with mean 0 and variance $2\nu\Delta t$. Define $\tilde{D}_{\Delta t} u^0$ by

$$\begin{aligned} \tilde{D}_{\Delta t} u^0(x, y) = U(x) &+ \sum_{j=1}^{N} \omega_j b_h(x - x_j) H(|y_j + \zeta_j| - y) \\ &+ \sum_{i=1}^{r} \sum_{l=1}^{q_i} \omega_{il} b_h(x - a_i) H(|\zeta_{il}| - y), \end{aligned} \tag{4.7}$$

where q_i and ω_{il} are chosen as in Algorithm A, Algorithm B, or by solving the no-slip boundary condition exactly at each a_i,

$$\sum_{l=1}^{q_i} \omega_{il} = -u^0(a_i, 0), \qquad i = 1, \cdots, r. \tag{4.8}$$

We let $E\tilde{D}_{\Delta t} u^0$ denote the expectation of $\tilde{D}_{\Delta t} u^0$ taken with respect to the random walks ζ_j, ζ_{il}, and

$$\operatorname{var}(\tilde{D}_{\Delta t} u^0) = E[(\tilde{D}_{\Delta t} u^0 - E\tilde{D}_{\Delta t} u^0)^2]$$

denote the variance of $\tilde{D}_{\Delta t} u^0$ with respect to these random walks.

We will obtain bounds in the $L^1(\Omega)$, $L^2(\Omega)$, and $L^\infty(\Omega)$ norms, where $\Omega = [0, L] \times [0, \infty)$ is our computational domain. For a function $f(x, y)$ defined on Ω we will sometimes need to consider the sup norm of f as a function defined on the wall alone,

$$\|f(\cdot, 0)\|_\infty \equiv \sup_{x \in [0, L]} |f(x, 0)|.$$

Furthermore, if f is piecewise C^1 on $[0, L]$ and C^1 on the open intervals (b_{i-1}, b_i), where $0 = b_1 \leqq \cdots \leqq b_m = L$ then, following Schultz [31, p. 2], we define

$$\|\partial_x f(\cdot, 0)\|_\infty \equiv \max_i \sup_{b_{i-1} \leqq x \leqq b_i} |\partial_x f(x, 0)|.$$

The L^2 norm of $f(x, 0)$ and $\partial_x f(x, 0)$ are defined similarly.

4.2. The analysis. We begin by showing that the exact solution $D_{\Delta t}u^0$ is the expected value of our random walk process when the no-slip boundary condition is solved exactly at each point on the wall.

THEOREM 4.1. *Let u^0 be given by* (4.4) *and let $D_{\Delta t}u^0$ denote the exact solution of* (2.2a)-(2.2b) *with initial data u^0. Let ζ, ζ_j be Gaussian-distributed random variables with mean* 0 *and variance $2\nu\Delta t$ and let E denote the expected value with respect to these random variables. Then*

$$D_{\Delta t}u^0(x,y) = E\left[U(x) + \sum_j \omega_j b_h(x-x_j) H(|y_j+\zeta_j|-y) - u^0(x,0) H(|\zeta|-y) \right]. \tag{4.9}$$

Proof. The exact solution to (2.2a)-(2.2b) on the half plane $y \geqq 0$ can be found by extending the initial data antisymmetrically about $x=0$,

$$u^0(x,y) \equiv -u^0(x,-y), \qquad y<0,$$

and solving the diffusion equation on the *entire* real line $-\infty < y < \infty$ with initial data u^0. We can write down the solution of this latter problem by using the fundamental solution of the heat equation on $\mathbb{R}$,

$$u(x,y,t) = \frac{1}{\sqrt{4\pi\nu t}} \int_{-\infty}^{\infty} \exp\left(\frac{-(y-s)^2}{4\nu t}\right) u^0(x,s)\, ds.$$

Now let $c_j = \omega_j b_h(x-x_j)$, where we have suppressed the dependence on x for notational convenience. Then

$$\begin{aligned}
D_{\Delta t}u^0(x,y) &= \frac{1}{\sqrt{4\pi\nu\Delta t}} \int_0^{\infty} \exp\left(\frac{-(y-s)^2}{4\nu\Delta t}\right)\left(U(x) + \sum_j c_j H(y_j - s)\right) ds \\
&\quad - \frac{1}{\sqrt{4\pi\nu\Delta t}} \int_{-\infty}^{0} \exp\left(\frac{-(y-s)^2}{4\nu\Delta t}\right)\left(U(x) + \sum_j c_j H(y_j + s)\right) ds \\
&= \frac{1}{\sqrt{4\pi\nu\Delta t}} \int_{-y}^{\infty} \exp\left(\frac{-\zeta^2}{4\nu\Delta t}\right) U(x)\, d\zeta \\
&\quad - \frac{1}{\sqrt{4\pi\nu\Delta t}} \int_{-\infty}^{-y} \exp\left(\frac{-\zeta^2}{4\nu\Delta t}\right) U(x)\, d\zeta \\
&\quad + \sum_j c_j \frac{1}{\sqrt{4\pi\nu\Delta t}} \int_{y-y_j}^{y} \exp\left(\frac{-\zeta^2}{4\nu\Delta t}\right) d\zeta \\
&\quad + \sum_j c_j \frac{1}{\sqrt{4\pi\nu\Delta t}} \int_{-y}^{-y-y_j} \exp\left(\frac{-\zeta^2}{4\nu\Delta t}\right) d\zeta \\
&= \frac{1}{\sqrt{4\pi\nu\Delta t}} \int_{-\infty}^{\infty} \exp\left(\frac{-\zeta^2}{4\nu\Delta t}\right) U(x)\, d\zeta \\
&\quad - \frac{2}{\sqrt{4\pi\nu\Delta t}} \int_{-\infty}^{-y} \exp\left(\frac{-\zeta^2}{4\nu\Delta t}\right) U(x)\, d\zeta \\
&\quad + \sum_j c_j \frac{1}{\sqrt{4\pi\nu\Delta t}} \int_{y-y_j}^{\infty} \exp\left(\frac{-\zeta^2}{4\nu\Delta t}\right) d\zeta \\
&\quad + \sum_j c_j \frac{1}{\sqrt{4\pi\nu\Delta t}} \int_{-\infty}^{-y-y_j} \exp\left(\frac{-\zeta^2}{4\nu\Delta t}\right) d\zeta \\
&\quad - \sum_j c_j \frac{1}{\sqrt{4\pi\nu\Delta t}} \int_{y}^{\infty} \exp\left(\frac{-\zeta^2}{4\nu\Delta t}\right) d\zeta - \sum_j c_j \frac{1}{\sqrt{4\pi\nu\Delta t}} \int_{-\infty}^{-y} \exp\left(\frac{-\zeta^2}{4\nu\Delta t}\right) d\zeta \\
&= U(x) + \sum_j c_j E[H(|y_j+\zeta|-y)] - u^0(x,0) E[H(|\zeta|-y)].
\end{aligned}$$

It is apparent from (4.9) that the amount by which $\tilde{D}_{\Delta t}u^0$ differs from $D_{\Delta t}u^0$ depends on how well we approximate $u^0(x,0)$ by creating new sheets at the wall. We now show that the maximum value of this difference is $O(h+\omega_{\max})$.

THEOREM 4.2. *Let u^0 and $\tilde{D}_{\Delta t}u^0$ be defined by* (4.4) *and* (4.7), *respectively. Then*

$$\|E\tilde{D}_{\Delta t}u^0 - D_{\Delta t}u^0\|_\infty \leqq \tfrac{1}{2}\|\partial_x u^0(\cdot,0)\|_\infty h + \omega_{\max}. \tag{4.10}$$

Proof. Let $u_i' = -\sum_{l=1}^{q_i}\omega_{il}$. Then, since ζ and the ζ_{il} are identically distributed, (4.7) and (4.9) imply that

$$E\tilde{D}_{\Delta t}u^0(x,y) - D_{\Delta t}u^0(x,y) = -\left[\sum_{i=1}^{r} u_i' b_h(x-a_i) - u^0(x,0)\right] EH(|\zeta|-y). \tag{4.11}$$

For all y, $|EH(|\zeta|-y)| \leqq 1$, and hence

$$\|E\tilde{D}_{\Delta t}u^0 - D_{\Delta t}u^0\|_\infty \leqq \left|\sum_{i=1}^{r} u_i' b_h(x-a_i) - u^0(x,0)\right|.$$

Define $u_i = u^0(a_i,0)$. By definition of the u_i' and one of (2.8), (2.9), or (4.8) we have

$$|u_i' - u_i| = |q_i\omega_i + u_i| < \omega_{\max}. \tag{4.12}$$

Note that for all x, $\sum_{i=1}^{r}|b_h(x-a_i)| = 1$. Therefore,

$$\begin{aligned}\left|\sum_{i=1}^{r} u_i' b_h(x-a_i) - u^0(x,0)\right| &\leqq \left|\sum_{i=1}^{r} u_i' b_h(x-a_i) - \sum_{i=1}^{r} u_i b_h(x-a_i)\right| \\ &\quad + \left|\sum_{i=1}^{r} u_i b_h(x-a_i) - u^0(x,0)\right| \\ &\leqq \omega_{\max} + \tfrac{1}{2}\|\partial_x u^0(\cdot,0)\|_\infty h,\end{aligned}$$

where we have used the fact that $\sum u_i b_h(x-a_i)$ is the piecewise linear interpolant of $u^0(x,0)$ with breaks at the a_i and Exercise 2.3 of Schultz [31] to obtain

$$\left|\sum_{i=1}^{r} u_i b_h(x-a_i) - u^0(\cdot,0)\right| \leqq \frac{1}{2}\|\partial_x u^0(\cdot,0)\|_\infty h. \tag{4.13}$$

We now prove that $\tilde{D}_{\Delta t}u^0$ is a consistent approximation to $D_{\Delta t}u^0$ in the L^1 norm.

THEOREM 4.3. *Let u^0 and $\tilde{D}_{\Delta t}u^0$ be defined by* (4.4) *and* (4.7), *respectively. Then*

$$\|E\tilde{D}_{\Delta t}u^0 - D_{\Delta t}u^0\|_1 \leqq \frac{L}{\sqrt{\pi}}\left\{\frac{1}{2}\|\partial_x u^0(\cdot,0)\|_\infty h + \omega_{\max}\right\}\sqrt{4\nu\Delta t}.$$

Proof. Let u_i and u_i' be as in the proof of Theorem 4.2. From (4.11) we obtain

$$\|E\tilde{D}_{\Delta t}u^0 - D_{\Delta t}u^0\|_1 = \int_0^L \left|\sum_{i=1}^{r} u_i' b_h(x-a_i) - u^0(x,0)\right| dx \int_0^\infty EH(|\zeta|-y)\, dy. \tag{4.14}$$

We use (4.12), (4.13), $rh = L$, and $\int_0^L |b_h(x-a_i)|dx = h$ to estimate the first integral on the right in (4.14):

$$\begin{aligned}\int_0^L \left|\sum_{i=1}^{r} u_i' b_h(x-a_i) - u^0(x,0)\right| dx &\leqq \int_0^L \left|\sum_{i=1}^{r} u_i' b_h(x-a_i) - \sum_{i=1}^{r} u_i b_h(x-a_i)\right| dx \\ &\quad + \int_0^L \left|\sum_{i=1}^{r} u_i b_h(x-a_i) - u^0(x,0)\right| dx \\ &\leqq L\omega_{\max} + \frac{L}{2}\|\partial_x u^0(\cdot,0)\|_\infty h.\end{aligned}$$

In order to estimate the second integral, we write

$$EH(|\zeta|-y)=\frac{1}{\sqrt{4\pi\nu\Delta t}}\int_{-\infty}^{\infty}H(|\zeta|-y)\exp\left(\frac{-\zeta^2}{4\nu\Delta t}\right)d\zeta=\int_{y/\sqrt{2\nu\Delta t}}^{\infty}\frac{2e^{-\zeta^2/2}}{\sqrt{2\pi}}d\zeta, \tag{4.15}$$

whereby

$$\int_0^{\infty}EH(|\zeta|-y)\,dy=\int_0^{\infty}\int_{y/\sqrt{2\nu\Delta t}}^{\infty}\frac{2e^{-\zeta^2/2}}{\sqrt{2\pi}}d\zeta\,dy=\frac{\sqrt{4\nu\Delta t}}{\sqrt{\pi}}\int_0^{\infty}\int_y^{\infty}e^{-\zeta^2/2}\,d\zeta\,dy=\frac{\sqrt{4\nu\Delta t}}{\sqrt{\pi}}.$$

The last equality follows from integration by parts with respect to y.

Next we prove the consistency of $\tilde{D}_{\Delta t}$ in the L^2 norm. This theorem will also help us establish a bound on the probability distribution of the error in the L^2 norm (Theorem 4.8).

THEOREM 4.4. *Let u^0 and $\tilde{D}_{\Delta t}u^0$ be defined by* (4.4) *and* (4.7), *respectively. Then*

$$\|E\tilde{D}_{\Delta t}u^0-D_{\Delta t}u^0\|_2\leqq\left(\frac{2(\sqrt{2}-1)}{\sqrt{\pi}}\right)^{1/2}\left\{\sqrt{L}\omega_{\max}+\frac{1}{\pi}\|\partial_x u^0(\cdot,0)\|_2 h\right\}(2\nu\Delta t)^{1/4}. \tag{4.16}$$

Proof. Again let u_i and u_i' be defined as in the proof of Theorem 4.2. From (4.11) we find

$$\|E\tilde{D}_{\Delta t}u^0-D_{\Delta t}u^0\|_2=\left(\int_0^L\left(\sum_{i=1}^r u_i'b_h(x-a_i)-u^0(x,0)\right)^2dx\right)^{1/2}\times\left(\int_0^{\infty}(EH(|\zeta|-y))^2\,dx\right)^{1/2}.$$

The right-hand side of (4.16) is the product of two one-dimensional norms. The first of these is

$$\left\|\sum_{i=1}^r u_i'b_h(\cdot-a_i)-u^0(\cdot,0)\right\|_2\leqq\left\|\sum_{i=1}^r u_i'b_h(\cdot-a_i)-\sum_{i=1}^r u_ib_h(\cdot-a_i)\right\|_2+\left\|\sum_{i=1}^r u_ib_h(\cdot-a_i)-u(\cdot,0)\right\|_2.$$

We can evaluate the first term on the right by using (4.12) and the fact that $\sum b_h(x-a_i)\leqq 1$ for all x:

$$\left\|\sum_{i=1}^r u_i'b_h(\cdot-a_i)-\sum_{i=1}^r u_ib_h(\cdot-a_i)\right\|_2\leqq\sqrt{L}\omega_{\max}.$$

To evaluate the second term we use Theorem 2.4 of Schultz [31] to bound the L^2 norm of the difference between $u^0(x,0)$ and its piecewise linear interpolant $\sum u_ib_h(x-a_i)$,

$$\left\|\sum_{i=1}^r u_ib_h(\cdot-a_i)-u^0(\cdot,0)\right\|_2\leqq\frac{1}{\pi}\|\partial_x u^0(\cdot,0)\|_2 h.$$

We evaluate the other expression on the right-hand side of (4.16) by using (4.15) and Lemma 1 of Hald [20] with $a=b=2\nu\Delta t$,

$$\left(\int_0^{\infty}(EH(|\zeta|-y))^2\,dy\right)^{1/2}=\left(\int_0^{\infty}\int_{y/\sqrt{2\nu\Delta t}}^{\infty}\frac{2e^{-\zeta^2/2}}{\sqrt{2\pi}}d\zeta\int_{y/\sqrt{2\nu\Delta t}}^{\infty}\frac{2e^{-\zeta^2/2}}{\sqrt{2\pi}}d\zeta\,dy\right)^{1/2}=\left(\frac{2(\sqrt{2}-1)}{\sqrt{\pi}}\right)^{1/2}(2\nu\Delta t)^{1/4}.$$

In order to establish a bound on $\operatorname{var} \tilde{D}_{\Delta t} u^0$ in the L^1 norm we will need the following two lemmas, both of which are generalizations of previous work by Hald. The first lemma is a straightforward extension of Lemma 1 in [20] and we refer the reader to it for details of the proof.

LEMMA 4.5. *For $y \geqq 0$ define*

$$F(y) = \frac{2}{\pi}(\sqrt{2} - e^{y^2/2})\left(\frac{\sqrt{\pi}}{\sqrt{2}} + \int_0^y e^{-\zeta^2/2}\, d\zeta\right) + \frac{2\sqrt{2}}{\pi}\int_y^{\sqrt{2}y} e^{\zeta^2/2}\, d\zeta. \tag{4.17}$$

Then $F(0) = (2-\sqrt{2})/\sqrt{\pi}$, $F(\infty) = 4/\sqrt{\pi}$, and, for all $y \in [0, \infty)$,

$$\frac{(2-\sqrt{2})}{\sqrt{\pi}} \leqq F(y) \leqq \frac{4}{\sqrt{\pi}}. \tag{4.18}$$

Furthermore, for all $y_j \geqq 0$ we have

$$F(y_j) = \int_0^\infty \int_y^\infty \frac{2e^{-(\zeta - y_j)^2/2}}{\sqrt{2\pi}}\, d\zeta \int_0^y \frac{2e^{-(\zeta - y_j)^2/2}}{\sqrt{2\pi}}\, d\zeta\, dy.$$

We also need to establish a bound on the L^1 norm of the variance of the independent summands $H(|y_j + \zeta_j| - y)$. Hald proved this lemma in [20] for the case when $y_j = 0$.

LEMMA 4.6. *Let $y_j \geqq 0$, $F(y_j)$ be defined by (4.17) and ζ be a Gaussian random variable with mean 0 and variance $2\nu\Delta t$. Then*

$$\int_0^\infty \operatorname{var} H(|y_j + \zeta| - y)\, dy \leqq F(y_j/\sqrt{2\nu\Delta t})\sqrt{2\nu\Delta t}.$$

Proof. First note that

$$EH(|y_j + \zeta| - y) = \frac{1}{\sqrt{4\pi\nu\Delta t}} \int_{-\infty}^\infty H(|y_j + \zeta| - y) \exp\left(\frac{-\zeta^2}{4\nu\Delta t}\right) d\zeta = P(|y_j + \zeta| \geqq y).$$

Hence, since $H(y)^2 = H(y)$ and $1 - P(a \geqq b) = P(a < b)$, we have

$$\operatorname{var} H(|y_j + \zeta| - y) = P(|y_j + \zeta| \geqq y) P(|y_j + \zeta| < y).$$

Furthermore,

$$\begin{aligned} P(|y_j + \zeta| \geqq y) &= \frac{1}{\sqrt{4\pi\nu\Delta t}} \int_{-\infty}^\infty H(|y_j + \zeta| - y) \exp\left(\frac{-\zeta^2}{4\nu\Delta t}\right) d\zeta \\ &= \frac{1}{\sqrt{4\pi\nu\Delta t}} \int_y^\infty \exp\left(\frac{-(\zeta - y_j)^2}{4\nu\Delta t}\right) d\zeta \\ &\quad + \frac{1}{\sqrt{4\pi\nu\Delta t}} \int_{-\infty}^{-y} \exp\left(\frac{-(\zeta - y_j)^2}{4\nu\Delta t}\right) d\zeta \\ &\leqq \frac{2}{\sqrt{4\pi\nu\Delta t}} \int_y^\infty \exp\left(\frac{-(\zeta - y_j)^2}{4\nu\Delta t}\right) d\zeta, \end{aligned}$$

since the Gaussian curve is centered at $\zeta = y_j$. Similarly,

$$P(|y_j + \zeta| < y) \leqq \frac{2}{\sqrt{4\pi\nu\Delta t}} \int_0^y \exp\left(\frac{-(\zeta - y_j)^2}{4\nu\Delta t}\right) d\zeta.$$

Now let $z_j = y_j/\sqrt{2\nu\Delta t}$. Then, using Lemma 4.5, we find

$$\begin{aligned}\int_0^\infty \operatorname{var} H(|y_j+\zeta|-y)\,dy &= \int_0^\infty P(|y_j+\zeta|\geqq y)P(|y_j+\zeta|<y)\,dy\\ &\leqq \int_0^\infty \left\{\frac{2}{\sqrt{4\pi\nu\Delta t}}\int_y^\infty \exp\left(\frac{-(\zeta-y_j)^2}{4\nu\Delta t}\right)d\zeta\right.\\ &\qquad \left.\times\frac{2}{\sqrt{4\pi\nu\Delta t}}\int_0^y \exp\left(\frac{-(\zeta-y_j)^2}{4\nu\Delta t}\right)d\zeta\right\}dy\\ &= \int_0^\infty\int_{y/\sqrt{2\nu\Delta t}}^\infty \frac{2e^{-(\zeta-z_j)^2/2}}{\sqrt{2\pi}}\,d\zeta\int_0^{y/\sqrt{2\nu\Delta t}}\frac{2e^{-(\zeta-z_j)^2/2}}{\sqrt{2\pi}}\,d\zeta\,dy\\ &= \sqrt{2\nu\Delta t}F(z_j).\end{aligned}$$

Our bound on the L^1 norm of the variance of $\tilde{D}_{\Delta t}u^0$ now follows easily.

THEOREM 4.7. *Let u^0 and $\tilde{D}_{\Delta t}u^0$ be given by* (4.4) *and* (4.7), *respectively. Then the inequality in* (4.3) *holds with*

$$C_\nu = \frac{4}{\sqrt{\pi}}\left\{\|\omega^0\| + \frac{2}{3}L\|u^0(\cdot,0)\|_\infty\right\}.$$

Proof. Since the ζ_j and ζ_{il} are independent, identically distributed random variables, we have

$$\begin{aligned}\|\operatorname{var}(\tilde{D}_{\Delta t}u^0)\|_1 &= \sum_j \omega_j^2\int_0^L b_h^2(x-x_j)\,dx\int_0^\infty \operatorname{var} H(|y_j+\zeta|-y)\,dy\\ &\quad + \sum_{i=1}^r\sum_{l=1}^{q_i}\omega_{il}^2\int_0^L b_h^2(x-a_i)\,dx\int_0^\infty \operatorname{var} H(|\zeta|-y)\,dy.\end{aligned}\tag{4.19}$$

Since $0\leqq b_h(x)\leqq 1$ for all x, we have

$$\sum_j \omega_j^2\int_0^L b_h^2(x-x_j)\,dx \leqq \omega_{\max}\sum_j|\omega_j|\int_0^L b_h(x-x_j)\,dx = \omega_{\max}\|\omega^0\|.$$

For the piecewise linear b_h we have

$$\int_0^L b_h^2(x-a_i)\,dx = h\int_{-1}^1 l^2(x)\,dx \leqq \frac{2}{3}h,$$

where l is defined by (3.2). By definition of the q_i and ω_i we find

$$\sum_{l=1}^{q_i}\omega_{il}^2 \leqq \omega_{\max}\sum_{l=1}^{q_i}|\omega_{il}| \leqq \omega_{\max}|u^0(a_i,0)| \leqq \omega_{\max}\|u^0(\cdot,0)\|_\infty.$$

Using Lemma 4.6, $rh = L$, and (4.18), we now obtain (4.3),

$$\|\operatorname{var}(\tilde{D}_{\Delta t}u^0)\|_1 \leqq F(\infty)\{\|\omega^0\| + \tfrac{2}{3}L\|u^0(\cdot,0)\|_\infty\}\sqrt{2\nu\Delta t}\,\omega_{\max} \leqq C_\nu\sqrt{2\nu\Delta t}\,\omega_{\max}.$$

It is apparent from (4.3) that the L^1 norm of var $\tilde{D}_{\Delta t}u^0$ goes to zero like $\sqrt{\nu}$. In other words, the statistical fluctuations in our random walk approximation to $D_{\Delta t}u^0$ diminish with diminishing ν. Furthermore, a careful inspection of the proof will reveal that the bound in (4.3) exhibits the correct dependence on ν, Δt, and $\omega_{\max}$. In other words, the bound is sharp. Also note that this proof relies on the independence of the

random walks. When sheet tagging is used this independence is lost since sheets with the same tag overlap. This loss of independence results in a term of the form

$$\int_0^L \int_0^\infty \sum_{j\neq l} \omega_j\omega_l b_h(x-x_j)b_h(x-x_l)E[H(|y_j+\zeta_j|-y)H(|y_l+\zeta_l|-y)]\,dy\,dx$$
$$-\int_0^L \int_0^\infty \sum_{j\neq l} \omega_j\omega_l b_h(x-x_j)b_h(x-x_l)E[H(|y_j+\zeta_j|-y)]E[H(|y_l+\zeta_l|-y)]\,dy\,dx,$$

being added to the right-hand side of (4.19). (Here the sum is over all sheets, new and old.) Since this term will, in general, not be negative it follows that the sheet tagging can in fact *increase* the variance. This observation is corroborated by the numerical results presented in § 5.7.

Finally, we derive a bound on the probability distribution of the error in the L^2 norm. Our proof is based on ideas found in the proof of Theorem 2 of Hald [20].

THEOREM 4.8. *Assume that* $h^2 \leqq \omega_{\max} \leqq 1$, *let* u^0 *and* $\tilde{D}_{\Delta t}u^0$ *be defined by* (4.4) *and* (4.7), *respectively, and define*

$$C_D = C_\nu + \frac{2(\sqrt{2}-1)}{\sqrt{\pi}}(\sqrt{L}+\pi^{-1}\|\partial_x u^0(\cdot,0)\|_\infty)^2.$$

Then for all $\gamma > 0$,

$$P(\|\tilde{D}_{\Delta t}u^0 - D_{\Delta t}u^0\|_2 \geqq \gamma\sqrt{\omega_{\max}}) \leqq C_D\sqrt{2\nu\Delta t}\,\gamma^{-2}. \tag{4.20}$$

Remark. By using the well-known inequality

$$E[Z] \leqq a\left(1+\sum_{r=1}^{\infty} P(Z \geqq ra)\right)$$

for all random variables $Z \geqq 0$ and real numbers $a \geqq 0$ (see [12]) we can use (4.20) to establish a bound on the expected value of the error in the L^2 norm,

$$E\|\tilde{D}_{\Delta t}u^0 - D_{\Delta t}u^0\|_2 \leqq (1+2C_D)\sqrt{\omega_{\max}}(2\nu\Delta t)^{1/4}.$$

Proof. Chebyshev's inequality (Feller [14, p. 151]) implies

$$P(\|\tilde{D}_{\Delta t}u^0 - D_{\Delta t}u^0\|_2 \geqq \gamma\sqrt{\omega_{\max}}) \leqq E[\|\tilde{D}_{\Delta t}u^0 - D_{\Delta t}u^0\|_2^2](\omega_{\max}\gamma^2)^{-1}.$$

Since $E(\tilde{D}_{\Delta t}u^0 - D_{\Delta t}u^0)^2 = \operatorname{var}(\tilde{D}_{\Delta t}u^0) + (E\tilde{D}_{\Delta t}u^0 - D_{\Delta t}u^0)^2$ we can use Fubini's theorem to obtain

$$E[\|\tilde{D}_{\Delta t}u^0 - D_{\Delta t}u^0\|_2^2] = \|\operatorname{var}\tilde{D}_{\Delta t}\|_1 + \|E\tilde{D}_{\Delta t}u^0 - D_{\Delta t}u^0\|_2^2.$$

The inequality in (4.20) now follows from Theorems 4.4 and 4.7, and our assumption that $h^2 \leqq \omega_{\max}$.

4.3. Remarks. Theorems 4.2, 4.3, and 4.4 state that our random walk approximation $\tilde{D}_{\Delta t}u^0$ to the solution $D_{\Delta t}u^0$ is consistent in the L^1, L^2, and L^∞ norms, respectively. The term in (4.10) that is $O(\omega_{\max})$ is due to our failure to satisfy the no-slip boundary condition exactly at the gridpoints a_i. The term that is $O(h)$ is due to using a piecewise linear interpolation to the tangential velocity $u^0(x, 0)$ at the wall. If we use a higher-order interpolation, the order of this last error increases. For example, with B-spline smoothing it is $O(h^2)$. However, numerical results [26] have demonstrated that B-spline smoothing does not lead to an appreciable improvement in the overall accuracy of the method (although it may reduce the total number of sheets in the flow). This is because, as with all Monte Carlo methods, the dominant source of error is that due to the random walk.

Assume for the moment that we have the necessary estimates for the splitting error, the error due to approximating $A_{\Delta t}$ by $\tilde{A}_{\Delta t}$, and the stability of $A_{\Delta t}$. Then, by individually considering the errors made at each timestep, we can use (4.20) and the assumption that $\Delta t = O(\omega_{\max}^{2/3})$ to prove that the expected value of the error in the L^2 norm after k time steps is $O(\Delta t) + O(\omega_{\max}^{1/3}) + O(h^q)$, where $q > 0$ would depend on our estimate of the error due to approximating $A_{\Delta t}$ by $\tilde{A}_{\Delta t}$. (For an example of this type of argument see § 3 of Puckett [25].) It has recently been shown that, for the free-space problem, the random vortex method converges like $O(\log N/\sqrt{N})$ in the L^2 norm (Long [24]). This corresponds to a rate of $\log (\omega_{\max})^{-1}\sqrt{\omega_{\max}}$ for the vortex sheet method. (The $\log N$ is most likely a spurious term introduced by the analysis.) Based on the above observations we believe that the dependence of the vortex sheet method on $\omega_{\max}$ is $O(\omega_{\max}^p)$ for some p, with $\frac{1}{3} \leqq p \leqq \frac{1}{2}$, and that it is very likely that $p = \frac{1}{2}$.

5. Numerical results.

5.1. The test problem. We model two-dimensional flow past a flat plate with a constant free-stream velocity, $U(x) \equiv U_0$. This is known as Blasius flow [30], [37]. Here we take $U_0 = 1$. This is a stationary flow that has the well-known similarity solution

$$u(x, y) = f'(\eta), \tag{5.1}$$

$$\eta = y/\sqrt{\nu x}, \tag{5.2}$$

where f satisfies the ODE

$$ff'' + 2f''' = 0, \tag{5.3a}$$

$$f(0) = 0, \quad f'(0) = 0, \quad f'(\infty) = 1. \tag{5.3b}$$

While we cannot write down f exactly, it is a simple matter to solve (5.3a)-(5.3b) numerically with great accuracy (White [37, p. 262]), thus obtaining an effectively exact solution.

Blasius flow is a solution of equations (1.1a)-(1.1e) over the semi-infinite flat plate, $0 < x < \infty$, $0 \leqq y < \infty$. There is a small neighborhood of the leading edge of the plate in which the transverse velocity component is of the same order of magnitude as the tangential velocity component; hence the Prandtl equations are not valid in this region. In order to ameliorate the effects of this leading edge singularity and to conveniently handle the downstream boundary condition, we consider the following periodic problem.

We compute over the portion of the plate from $a = 3h$ to $b = 1 + 3h$. We map physical space, $\Omega \equiv \{(x, y)\colon x > 0, \text{ and } y \geqq 0\}$, onto the periodic domain $\Omega_C \equiv \{(x, y)\colon 3h \leqq x \leqq 1 + 3h, \text{ and } y \geqq 0\}$ by the transformation $(x, y) \in \Omega \to (x^*, y^*) \in \Omega_C$, where

$$x^* = x \bmod 1, \tag{5.4a}$$

$$y^* = y\sqrt{x^*/x}. \tag{5.4b}$$

Sheets whose centers move to the right of $x = b$ have their centers transformed according to (5.4a)-(5.4b) so that they now appear to lie near the beginning of Ω_C. Similarly, sheets that move backward, to the left of $x = a$, are rescaled and placed at the end of Ω_C. Furthermore, when calculating the velocity of a point that lies within one sheet length of the edge of our computational domain we take care to include the influence of sheets that lie near the other end. Thus we have eliminated the effects of the leading edge singularity by imposing as an upstream boundary condition the computed velocity profile that results from identifying $x = a$ and $x = b$ with appropriately scaled y

coordinates. This also eliminates spurious effects due to throwing sheets away after they pass $x = b$ (e.g., [9, p. 433]).

One drawback of the periodic formulation of this problem is that the total number of vortex elements in the flow increases with time. Once a sheet is created, it exists for the remainder of the computer calculation. Therefore the amount of vorticity above a given portion of the plate also increases with time. For Blasius flow this is nonphysical. It is our contention, however, that this is a good test of the algorithm's effectiveness. Vorticity creation is an important phenomenon and we would like to approximate it as accurately as possible. Successful strategies for minimizing the error here will lead to a better overall algorithm.

All results shown here are at time $T = 2$ with $\nu = 10^{-4}$. We used the piecewise linear cutoff (3.2) and initial data (2.14) with $U_{\max} = 1$.

5.2. Measurement of the error. In order to eliminate the dependence of the L^p norm of the error on the viscosity for $1 \leqq p < \infty$, we measure all such norms in the transformed variables (x, η),

$$\|u - \tilde{u}\|_p = \left(\int_a^b \int_0^\infty |u(x, \eta) - \tilde{u}(x, \eta)|^p \, d\eta \, dx \right)^{1/p}, \tag{5.5}$$

where η is given by (5.2). Furthermore, for $p = 1$ we divide the error in the L^1 norm by

$$\|1 - u\|_1 = \int_a^b \int_0^\infty (1 - f'(\eta)) \, d\eta \, dx = (\eta - f(\eta))\Big|_{\eta=0}^{\eta=\infty} \approx 1.7208$$

(see [30], p. 130) and report the "normalized" error:

$$\|u - \tilde{u}\|_1 / \|1 - u\|_1 .$$

To estimate the integral norm in (5.5) we used

$$\begin{aligned} \|u - \tilde{u}\|_p &\approx \left(\sum_{i=1}^r h \int_0^\infty |u(a_i, \eta) - \tilde{u}(a_i, \eta)|^p \, d\eta \right)^{1/p} \\ &= h^{1/p} \left(\sum_{i=1}^r (\sqrt{\nu a_i})^{-1} \int_0^\infty |u(a_i, y) - \tilde{u}(a_i, y)|^p \, dy \, dx \right)^{1/p}. \end{aligned}$$

The one-dimensional error above a_i was calculated using the trapezoid rule

$$\int_0^\infty |u(a_i, y) - \tilde{u}(a_i, y)|^p \, dy \approx \sum_j ((\mathrm{err}_j)^p + (\mathrm{err}_{j+1})^p) \frac{(y_{j+1} - y_j)}{2}, \tag{5.6}$$

where $\mathrm{err}_j = |u(a_i, y_j) - \tilde{u}(a_i, y_j)|$, the sum is only over those y_j such that

$$b_h(a_i - x_j) \neq 0, \tag{5.7}$$

and we have ordered the y_j so that $y_j \leqq y_{j+1}$ for all j. In other words, we use a grid that corresponds to the location of the sheets above a_i. To ensure that the sum in (5.6) starts at $y = 0$, we place a sheet with no weight at $(a_i, 0)$. The value of $u(a_i, y_j) = f'(y_j/\sqrt{\nu a_i})$ was determined by linear interpolation from an array containing values of f' at equally spaced points $\eta = 0.0, 0.01, \cdots, 8.0$. We estimate the sup norm of the error similarly,

$$\|u - \tilde{u}\|_\infty \approx \max \{|u(a_i, y_j) - \tilde{u}(a_i, y_j)|\},$$

where the max is taken over all i, j satisfying (5.7).

The velocity, vorticity, drag, and each of the various norms of the error are random variables. We therefore make several different runs, which we refer to as *trials*. Each

trial has a different starting seed for the random number generator. We estimate the expected value of a randomly varying quantity Θ by $\bar{\Theta}$, where

$$\bar{\Theta} = \frac{1}{n} \sum_{i=1}^{n} \Theta_i \tag{5.8}$$

and Θ_i is the value of Θ calculated from the ith trial. We estimate the standard deviation of Θ by

$$\tilde{\sigma} = \frac{1}{\sqrt{n-1}} \left(\sum_{i=1}^{n} (\Theta_i - \bar{\Theta})^2 \right)^{1/2}. \tag{5.9}$$

We will also have occasion to refer to the *standard error* σ_Θ of the estimate in (5.8) defined by

$$\sigma_\Theta = \frac{\sigma}{\sqrt{n}} \tag{5.10}$$

([22, p. 21]), where σ is the true standard deviation for the parent distribution of the Θ_i. The quantity σ_Θ is simply the standard deviation of the distribution of the $\bar{\Theta}$'s and is therefore a measure of how good an estimate (5.8) is of the true mean. Since we do not know σ we will use (5.10) with σ replaced by $\tilde{\sigma}$ from (5.9). Unless noted otherwise, all of the data below are estimates based on $n = 25$ trials.

5.3. An estimate of the rate of convergence. We begin by presenting numerical results which demonstrate that the vortex sheet method converges when it is used to model the Blasius flow. Table 1 contains $\bar{\Theta}$ and $\tilde{\sigma}$ for the (normalized) L^1 norm of the error. In all runs displayed here $\Delta t = h/U_{\max}$. Note that as we move down a column the error eventually levels out. Since Δt and h are constant along columns it follows that the error which decreases along the columns is due to $\omega_{\max}$ alone. The "plateau" at the bottom of the column is due to those sources of error that depend on Δt and h. Similarly, it is apparent that for fixed values of $\omega_{\max}$ the error decreases with decreasing h, provided $\omega_{\max} < h^2/2L\Delta t$. This corresponds to $C_0 < 1/2L$ in (2.15). However, after leveling off the error *begins to increase* when this condition is violated. We observed this phenomenon consistently in all of our runs; it occurred with both the piecewise linear and B-spline cutoffs. We will investigate this behavior more thoroughly in § 5.5 below.

TABLE 1
Discrete L^1 norm of the error. Estimated mean and standard deviation of the error.

	h $(\Delta t = h/U_{\max})$			
$\omega_{\max}$	5^{-1}	10^{-1}	20^{-1}	40^{-1}
5^{-1}	0.4002 ± 0.0734	—	—	—
10^{-1}	0.2989 ± 0.0638	0.2983 ± 0.0521	—	—
20^{-1}	0.2580 ± 0.0475	0.2239 ± 0.0399	0.2230 ± 0.0279	—
40^{-1}	0.2663 ± 0.0473	0.1773 ± 0.0239	0.1657 ± 0.0112	0.1903 ± 0.0165
80^{-1}	0.2483 ± 0.0243	0.1636 ± 0.0202	0.1267 ± 0.0126	0.1346 ± 0.0101
160^{-1}	0.2529 ± 0.0252	0.1594 ± 0.0104	0.1088 ± 0.0103	0.0990 ± 0.0075
320^{-1}	0.2473 ± 0.0146	0.1528 ± 0.0093	0.1007 ± 0.0069	0.0778 ± 0.0077[1]
640^{-1}	0.2511 ± 0.0088	0.1534 ± 0.0068	0.0806 ± 0.0075	0.0627 ± 0.0060[2]

[1] Here $n = 16$, where n is the number of trials.
[2] $n = 2$.

In Fig. 1 we plot the log of the errors in Table 1 versus $\log h^{-1}$ for various relationships between $\omega_{\max}$ and h. The first data point in each sequence is $h = 5^{-1}$ and $\omega_{\max} = 10^{-1}$. For h fixed the abscissa corresponds to $\omega_{\max} = 10^{-1}, \cdots, 80^{-1}$. (For $\omega_{\max}$ fixed the last two data points are not displayed in Table 1.) When $\omega_{\max} = O(h^2)$ the resulting curve is nearly linear. This indicates that the error due to $\omega_{\max}$ is decreasing at least as fast as that due to h. We can attempt to discern a dependence of the error on h of the form error $= O(h^q)$ from this data. The slope of the line connecting the first and last points of the bottommost curve is $-0.7510 \approx -\frac{3}{4}$, implying $q \approx \frac{3}{4}$. However, if instead we choose the data from the last row of Table 1 (the error due to $\omega_{\max}$ should be very small here), then we find $q \approx \frac{2}{3}$. There is not enough data here to determine q beyond all doubt. We conjecture $q \geqq \frac{2}{3}$ and wonder why there is no evidence for $q = 1$. In Fig. 2 we plot the standard deviations that correspond to the data in Fig. 1. The

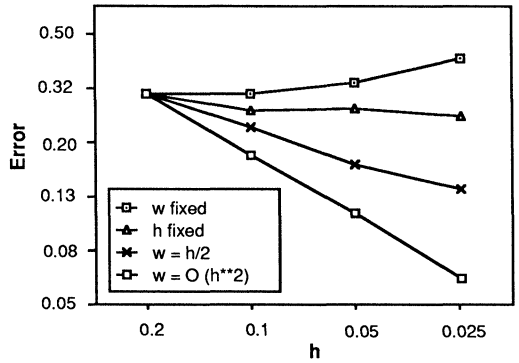

FIG. 1. Log $\bar{\Theta}$ *versus* log $1/h$.

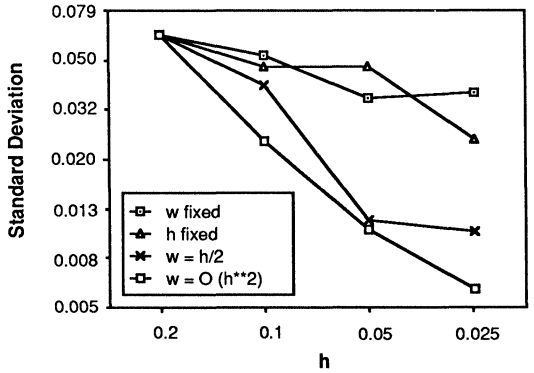

FIG. 2. Log $\tilde{\sigma}$ *versus* log $1/h$.

nearly linear decay of the lowest curve again indicates that when $\omega_{\max} = O(h^2)$ the error due to $\omega_{\max}$ decreases at least as rapidly as that due to h.

We repeated this experiment with the timestep halved, $\Delta t = h/2U_{\max}$, in an effort to determine if any of the errors would decrease when Δt alone was decreased. These errors, presented in Table 2, were remarkably close to those in Table 1, sometimes agreeing to several decimal places. Furthermore, many of these new errors lie within three standard errors of the values in Table 1 (using $\tilde{\sigma}$ from either table), making the two quantities statistically indistinguishable from each other. This was also true for the errors in the L^2 norm. We conclude that the errors presented in Table 1 do not diminish when h and $\omega_{\max}$ are fixed and Δt is decreased. This indicates that the errors due to temporal discretization are much smaller than the other sources of error. This may be because we are computing a stationary flow, and we caution the reader against drawing conclusions for more general flows.

We made a sequence of runs under the assumption that the error is $O(\sqrt{\omega_{\max}}) + O(h^{2/3})$. We set $h = O(\omega_{\max}^{3/4})$, $\Delta t = h/U_{\max}$, and, starting with $\omega_{\max} = 0.025$ and $h = 0.2$, made five runs decreasing $\omega_{\max}$ by two on each run. The results appear in Table 3. Note that the errors here are the results after only one trial, rather than being our estimate of the expected value $\bar{\Theta}$.

The column labeled "time" contains the time in CPU minutes it took for one trial on a CRAY X-MP. The FORTRAN program was designed to be as fast as possible. In particular, we vectorized every loop that would admit vectorization. We also employed a "bin" data structure in which all sheets lying in $a_i - h/2 \leqq x < a_i + h/2$ are kept in the same bin. Thus, to compute the velocity of a sheet in the ith bin we need only loop over those sheets in adjacent bins. Hence, instead of every sheet interacting

TABLE 2

Discrete L^1 norm of the error. The errors in Table 1 do not decrease as Δt is decreased with h and $\omega_{\max}$ left fixed.

	h $(\Delta t = h/2U_{\max})$			
$\omega_{\max}$	5^{-1}	10^{-1}	20^{-1}	40^{-1}
5^{-1}	0.4318 ± 0.0733	—	—	—
10^{-1}	0.3215 ± 0.0762	0.2967 ± 0.0469	—	
20^{-1}	0.2762 ± 0.0670	0.2336 ± 0.0310	0.2463 ± 0.0331	—
40^{-1}	0.2721 ± 0.0502	0.1787 ± 0.0256	0.1778 ± 0.0134	0.2170 ± 0.0167
80^{-1}	0.2402 ± 0.0351	0.1586 ± 0.0232	0.1276 ± 0.0158	0.1498 ± 0.0096

TABLE 3

(One trial per row.) A convergence study with $h = O(\omega_{\max}^{3/4})$ and $\Delta t = h/U_{\max}$.

$\omega_{\max}$	L^1 norm	L^2 norm	L^∞ norm	Sheets	Time	δ_1 av	δ_2 av
40^{-1}	0.2817	0.2489	0.2708	226	0.002	0.0044	0.00161
80^{-1}	0.1617	0.1756	0.2677	939	0.022	0.0024	0.00070
160^{-1}	0.1044	0.1070	0.1536	2954	0.218	0.0013	0.00037
320^{-1}	0.0823	0.0915	0.2719	13755	3.638	0.0009	0.00029
640^{-1}	0.0592	0.0631	0.1141	37206	31.131	0.0007	0.00019

with every other sheet in the advection step, for a total of N^2 interactions, each sheet has approximately $3hN$ interactions. This results in an algorithm that is approximately $O(3hN^2)$. (The actual amount of work depends on how uniformly the sheets are distributed along the plate.)

We also measured the error in approximating the *displacement thickness* and *momentum thickness.* The displacement thickness above x, $\delta_1(x)$, defined by

$$\delta_1(x) = \int_0^\infty \left(1 - \frac{u(x, y)}{U(x)}\right) dy$$

is the amount by which a streamline has been displaced by the thickening of the boundary layer from the beginning of the plate to x. The momentum thickness above x, $\delta_2(x)$, defined by

$$\delta_2(x) = \int_0^\infty \frac{u(x, y)}{U(x)} \left(1 - \frac{u(x, y)}{U(x)}\right) dy$$

is a measure of the amount of momentum that has been lost due to the boundary layer. See Schlichting [30] or White [37] for more details.

We measured the average error in these quantities along the wall as follows. The average error in the *displacement thickness* $\delta_1 av$ is defined by

$$\delta_1 av = \frac{1}{r} \sum_{i=1}^{r} |\delta_1(a_i) - \tilde{\delta}_1(a_i)|, \tag{5.11}$$

where $\tilde{\delta}_1$ is the trapezoid rule approximation to δ_1 given by (5.6) with $u(a_i, y)$ replaced with 1. Similarly, $\delta_2 av$ is the average error in the momentum thickness defined by (5.11) with δ_1 and $\tilde{\delta}_1$ replaced by δ_2 and $\tilde{\delta}_2$, where $\tilde{\delta}_2$ is the trapezoid rule approximation to δ_2. Note that we have not scaled out the effect of ν in our calculation of $\tilde{\delta}_1$ and $\tilde{\delta}_2$ and hence, $\delta_1 av$ and $\delta_2 av$ are $O(\sqrt{\nu}) = O(10^{-2})$.

In Fig. 3 we compare the L^1 error from Table 3 with the conjectured rate of convergence. It is apparent that for this choice of parameters the L^1 error *on the average*

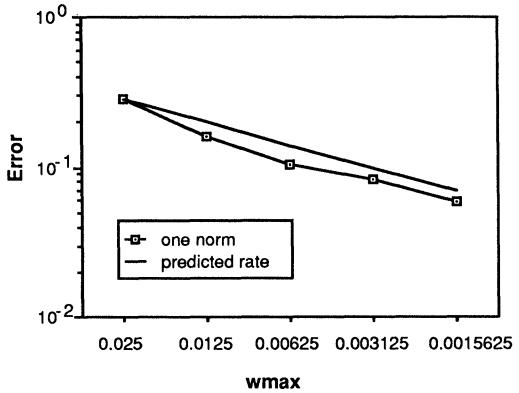

FIG. 3. *Actual versus predicted rate.*

decreases at a rate close to the anticipated one. In other words, the error may decrease by more or less than $\sqrt{2}$ from one row to the next, but from the first row to the last row the error has decreased by approximately a factor of 4. These remarks also apply to the L^2 error and the average error in the momentum and displacement thicknesses. The L^∞ norm was not as well behaved. This is not surprising since for random walk methods there can be small sets (in (x, y)-space) on which the error is large (e.g., Hald [20, § 5]). Of course the integral norms ameliorate the effects of large errors on small sets.

Our goal here has been to demonstrate that we need not average to use effectively these random walk methods. The fact that most of the results reported on in this paper are averages should not be construed as suggesting that we must always "ensemble average" to get reasonable results. It is apparent from Table 3 that we can make one run as long as it is in a regime of small variance. Based on our experience this can best be accomplished by ensuring that $\omega_{\max}$ is always small compared to $h^2/L\Delta t$ and by decreasing $\omega_{\max}$ faster than h and Δt. Here we have chosen $\omega_{\max} \leqq h^2/8L\Delta t$, which corresponds to $C_0 = L/8$ in (2.15) and let $\omega_{\max} = O(h^{4/3})$. In general we recommend taking $\omega_{\max} = O(h^{2q})$ with $\frac{2}{3} \leqq q \leqq 1$. Our experience with $q > \frac{2}{3}$ has not produced as consistently good results as those shown here, but we do not have enough evidence to unequivocally state that the optimal choice of q is $\frac{2}{3}$.

5.4. Second-order integration in time. Next we investigate the effect of solving (2.7a), (2.7b) with a second-order ODE solver. We conduct the same experiment as in Table 1 but with (2.6a), (2.6b) replaced by

$$x_j^{k+1/2} = x_j^k + \Delta t \tilde{u}_{1/2}(x_j', y_j'), \qquad y_j^{k+1/2} = y_j^k + \Delta t \tilde{v}_{1/2}(x_j', y_j')$$

where

$$x_j' = x_j + \frac{\Delta t}{2}\tilde{u}^k(x_j^k, y_j^k), \qquad y_j' = y_j + \frac{\Delta t}{2}\tilde{v}^k(x_j^k, y_j^k)$$

is the position of the jth sheet after one half of a timestep and $(\tilde{u}_{1/2}, \tilde{v}_{1/2})$ is the velocity field induced by the sheets when their centers are at these positions. Comparing these results with Table 1, we observe no increase in accuracy over Euler's method solution of (2.7a), (2.7b). This is consistent with the results displayed in Table 2. Of course we did not use second-order operator splitting (i.e., Strang splitting), and hence do not expect to see all sources of error that depend on Δt decrease. Nonetheless, there appears to be no improvement in the error due to second-order time discretization. It is instructive to compare these results with the effect of using second-order time integration in a one-dimensional random particle method as shown in Tables 3 and 4 of [25].

TABLE 4
Discrete L^1 norm of the error. Second-order integration in time.

	h $(\Delta t = h/U_{\max})$			
$\omega_{\max}$	5^{-1}	10^{-1}	20^{-1}	40^{-1}
5^{-1}	0.4224 ± 0.0995	—	—	—
10^{-1}	0.3290 ± 0.1044	0.3183 ± 0.0494	—	—
20^{-1}	0.2736 ± 0.0551	0.2316 ± 0.0276	0.2547 ± 0.0285	—
40^{-1}	0.2261 ± 0.0425	0.1701 ± 0.0227	0.1759 ± 0.0201	0.2271 ± 0.0204
80^{-1}	0.2325 ± 0.0285	0.1552 ± 0.0225	0.1323 ± 0.0128	0.1537 ± 0.0114

It is unclear to what extent this lack of dependence on the timestep is due to the stationary character of the test problem. Nevertheless, we feel compelled to make several comments regarding second-order time integration. There seems to be a prevalence of opinion among users of hybrid vortex sheet/vortex blob methods that the use of a higher-order time integration will result in a better solution. Presumably this opinion is based on theoretical results for the vortex method solution of Euler's equations with higher-order time integration (e.g., [1], [21]). However, the following points should be made in regard to the vortex sheet method: (i) A second-order scheme takes in twice as much work. (ii) We are constrained by (2.13) to decrease Δt as rapidly as h. (iii) Our results indicate that for the Blasius flow problem the dominant sources of error are those that depend on h and $\omega_{\max}$. Hence, we may be doing twice as much work for a negligible gain in accuracy. The first two considerations also apply when the vortex sheet method is used to model other flows. We note that, for somewhat different reasons, Sethian [33] has also questioned the effectiveness of using a second-order time-integration scheme with the vortex sheet method.

5.5. The behavior of the algorithm with decreasing h. Let us consider the dependence of N on $\omega_{\max}$. For example, assume that $\omega_{\max}$ divides $U_{\max}=1$ evenly and let the initial data be given by (2.14). Let N_x denote the number of sheets above x. Then at the first timestep we have $N_{a_i}=\omega_{\max}^{-1}$ for each gridpoint a_i on the wall. In general, at least for reasonable pressure gradients (UU_x small), we expect that $N_x=O(\omega_{\max}^{-1})$ for any x. In Table 5 we show the average number of sheets in the flow at time $T=2.0$ as a function of $\omega_{\max}$, h, and Δt.[1] It is apparent that if $\omega_{\max}$ is decreased by 2 with h and Δt fixed, then the average number of sheets does not increase by significantly more than 2.

TABLE 5

Discrete L^1 norm of the error. Gradual increase of the L^1 error for decreasing h, Δt, and fixed $\omega_{\max}$.

	h ($\Delta t = h/U_{\max}$)							
$\omega_{\max}$	0.2		0.1		0.05		0.025	
	Sheets	Error	Sheets	Error	Sheets	Error	Sheets	Error
0.2	26	0.4317	63	0.4449	179	0.5434	880	0.6860
0.1	54	0.3106	125	0.2915	328	0.3331	1074	0.4169
0.05	109	0.2724	253	0.2054	641	0.2317	1986	0.2858
0.025	222	0.2524	498	0.1681	1248	0.1630	3702	0.1989

We would also expect that letting h go to $h/2$ with $\omega_{\max}$ fixed would produce similar results. This turns out not to be the case. It is apparent from Table 5 that under these circumstances the average number of sheets in the flow always increases by *more* than 2, often by much more. Since $\Delta t = h/U_{\max}$ in all these runs, we can inquire if this unexpected increase is due to the increased number of timesteps as we decrease Δt. To answer this question we made a sequence of runs fixing $\Delta t = 0.0125$ and reducing h as before. The results appear in Table 6. It is apparent that the average number of

[1] Some of the numbers here differ from those in Table 1 even though the choice of parameters is the same. This is because these trials were made on a different computer with a different random number generator.

TABLE 6
Discrete L^1 norm of the error. Gradual increase of the L^1 error for decreasing h and fixed Δt, $\omega_{\max}$.

	h ($\Delta t = 0.0125$)							
$\omega_{\max}$	0.2		0.1		0.05		0.025	
	Sheets	Error	Sheets	Error	Sheets	Error	Sheets	Error
0.2	31	0.4380	79	0.4489	242	0.5339	1056	0.7514
0.1	64	0.3640	158	0.3110	451	0.3647	1427	0.4549
0.05	128	0.2849	320	0.2310	909	0.2549	2745	0.3228
0.025	246	0.2733	612	0.1789	1712	0.1839	4978	0.2167

sheets continues to grow by significantly more than 2 as we move to the right along a row. Therefore, this phenomenon is not due to decreasing Δt.

Note that the factor by which the number of sheets grows is largest in the upper right-hand corner in both Tables 5 and 6. These regions also display an increase in the error as h is decreased with $\omega_{\max}$ left fixed. Both phenomena may be due to the fact that (2.15) is being violated. However we can make no definite assertion. We do note however that an abnormal growth in the number of sheets seems to characterize those regions of parameter space that have large errors. We consider this important for several reasons. The amount of work to compute the velocity at each of the sheets is at best $O(hN^2)$. Thus, since decreasing h results in many more sheets than decreasing $\omega_{\max}$ by the same amount, it also results in a more expensive computation. For the same reason decreasing h leads to a larger value of $\|\tilde{\omega}\|$, whereas decreasing $\omega_{\max}$ does not significantly alter $\|\tilde{\omega}\|$. Consequently, the bounds in § 4.2 that depend on $\|\omega^0\|$ deteriorate when h is decreased. Unfortunately, we cannot pursue a strategy of only decreasing $\omega_{\max}$; eventually there is no improvement, except possibly a reduction in the variance. It is therefore necessary to toe a fine line between decreasing h too rapidly and not decreasing h fast enough.

5.6. A comparison of particle-creation algorithms. In this section we present the results of a numerical experiment designed to compare the two particle-creation algorithms described in § 2.3.2. We obtained the errors in Table 7 with creation Algorithm A using a value of $\varepsilon = 10^{-6}$. Table 8 is a duplicate of Table 7, except here

TABLE 7
Discrete L^2 norm of the error. Average number of sheets and mean of the error using Algorithm A.

	h ($\Delta t = h/U_{\max}$)							
$\omega_{\max}$	0.2		0.1		0.05		0.025	
	Sheets	Error	Sheets	Error	Sheets	Error	Sheets	Error
0.2	60	0.3600	—	—	—	—	—	—
0.1	88	0.2957	289	0.2738	—	—	—	—
0.05	145	0.2525	422	0.2166	1407	0.2310	—	—
0.025	255	0.2327	676	0.1783	2021	0.1690	7060	0.1965
0.0125	477	0.2021	1150	0.1400	3109	0.1164	9835	0.1362

TABLE 8
Discrete L^2 norm of the error. Average number of sheets and mean of the error using Algorithm B.

	h ($\Delta t = h/U_{\max}$)							
$\omega_{\max}$	0.2		0.1		0.05		0.025	
	Sheets	Error	Sheets	Error	Sheets	Error	Sheets	Error
0.2	27	0.3610	—	—	—	—	—	—
0.1	53	0.2763	124	0.2766	—	—	—	—
0.05	109	0.2410	251	0.2090	638	0.2087	—	—
0.025	216	0.2378	495	0.1709	1256	0.1612	3749	0.1808
0.0125	430	0.2222	972	0.1549	2370	0.1258	6775	0.1329

we used creation Algorithm B, i.e., the same algorithm used for all other experiments in this paper. Note that here the errors are in the discrete L^2 norm. In all instances Algorithm A results in an increase in the number of sheets in the flow but with little or no improvement in accuracy. We also tried replacing $\varepsilon = 10^{-6}$ with $\varepsilon = \omega_{\max}/2$ and observed a similar result: there was no noticeable improvement in the error but more sheets than with Algorithm B. We conclude that Algorithm B is more efficient and recommend that all users of the vortex sheet method employ it.

5.7. Sheet tagging. Finally, we made a sequence of runs to examine the effectiveness of the sheet-tagging procedure. In Table 9 we present $\bar{\Theta}$ and $\tilde{\sigma}$ for the error in the L^1 norm. These figures should be compared with Table 1. It is apparent that the sheet tagging leads to neither a decrease in the error nor a reduction in the variance. We do not recommend the sheet-tagging procedure.

TABLE 9
Discrete L^1 norm of the error. Sheet tagging.

	h ($\Delta t = h/U_{\max}$)			
$\omega_{\max}$	0.2	0.1	0.05	0.025
0.2	0.5508 ± 0.2671	—	—	—
0.1	0.4574 ± 0.1933	0.3677 ± 0.1938	—	—
0.05	0.2922 ± 0.1145	0.2524 ± 0.0748	0.2844 ± 0.0777	—
0.025	0.2422 ± 0.1236	0.1729 ± 0.0399	0.2026 ± 0.0437	0.2045 ± 0.0236
0.0125	0.2406 ± 0.0893	0.1638 ± 0.0637	0.1413 ± 0.0308	0.1490 ± 0.0179

5.8. Conclusions. We have proved that one timestep of the random walk and sheet-creation process is a consistent approximation to the exact solution of the heat equation subject to the no-slip boundary condition. This is true in each of the L^1, L^2, and L^∞ norms. Furthermore, it follows from the proof that the truncation error is entirely due to our failure to satisfy the no-slip boundary condition exactly at each point on the boundary.

We have demonstrated numerically that the vortex sheet method converges when it is used to approximate Blasius flow, provided certain conditions on the computational parameters are satisfied. These include two accuracy conditions of the form $\Delta t U_{\max} \leqq h$

and $\omega_{\max} \leqq C_0 h^2/\Delta t$, where $C_0 = O(1/L)$ and a relative rate of refinement condition $\omega_{\max} = O(h^{2q})$ for some q with $2/3 \leqq q \leqq 1$. We have also shown that the error will eventually increase when the second condition is not satisfied; for example, this occurs when h goes to zero much faster than $\omega_{\max}$.

We have been unable to observe any improvement in the accuracy of the method when a second-order time-integration scheme is used, or when the other parameters are fixed and the timestep is decreased. This may be because the test problem is a stationary flow. However, we suggest workers carefully consider the advantages and disadvantages of a second-order time-integration scheme before using one with the vortex sheet method.

We have also demonstrated that the most efficient sheet-creation algorithm is one for which all sheet strengths have equal magnitude, $|\omega_j| = \omega_{\max}$. Algorithms that create sheets with varying magnitudes end up producing more sheets without improving the accuracy of the method. Finally, we have shown that the sheet-tagging procedure is not an effective variance-reduction technique and therefore should not be used.

Acknowledgments. The author would like to thank Alexandre Chorin and Ole Hald for their time, support, and encouragement. He also would like to acknowledge fruitful discussions with Phil Colella, Maciej Pindera, and Jamie Sethian.

REFERENCES

[1] C. R. ANDERSON AND C. A. GREENGARD, *On vortex methods*, SIAM J. Numer. Anal., 22 (1985), pp. 413–440.

[2] J. T. BEALE AND A. MAJDA, *Vortex methods* I: *Convergence in three dimensions*, Math. Comp., 39 (1982), pp. 1–27.

[3] ———, *Vortex methods* II: *higher order accuracy in two and three dimensions*, Math. Comp., 39 (1982), pp. 29–52.

[4] CARL DE BOOR, *A Practical Guide to Splines*, Springer-Verlag, New York, 1978.

[5] A. Y. CHEER, *A study of incompressible 2-D vortex flow past a circular cylinder*, SIAM J. Sci. Statist. Comput., 4 (1983), pp. 685–705.

[6] ———, *Unsteady separated wake behind an impulsively started cylinder in slightly viscous fluid*, unpublished manuscript, University of California, CA, 1986.

[7] Y. CHOI, J. A. C. HUMPHREY, AND F. S. SHERMAN, *Random vortex simulation of transient wall-driven flow in a rectangular enclosure*, J. Comp. Phys., 75 (1988), pp. 359–383.

[8] A. J. CHORIN, *Numerical study of slightly viscous flow*, J. Fluid Mech., 57 (1973), pp. 785–796.

[9] ———, *Vortex sheet approximation of boundary layers*, J. Comp. Phys., 27 (1978), pp. 428–442.

[10] A. J. CHORIN AND J. E. MARSDEN, *A Mathematical Introduction to Fluid Mechanics*, Springer-Verlag, New York, 1979.

[11] A. J. CHORIN, *Vortex models and boundary layer instability*, SIAM J. Sci. Statist. Comput., 1 (1980), pp. 1–21.

[12] K. L. CHUNG, *A Course in Probability Theory*, Harcourt, Brace, and World, New York, 1974.

[13] G. H. COTTET, *Convergence of a vortex in cell method for the two dimensional Euler equations*, Rapport Interne 108, Centre de Mathématiques Appliquées, École Polytechique, Paris, 1984.

[14] W. FELLER, *An Introduction to Probability Theory and its Applications*, 2nd ed., Vol. II, John Wiley, New York, 1971.

[15] A. F. GHONIEM, A. J. CHORIN, AND A. K. OPPENHEIM, *Numerical modeling of turbulent flow in a combustion tunnel*, Philos. Trans. Roy. Soc. London Ser. A, 304 (1982), pp. 303–325.

[16] J. GOODMAN, *Convergence of the random vortex method in two dimensions*, Commun. Pure Appl. Math., 40 (1987), pp. 189–220.

[17] C. A. GREENGARD, *Three dimensional vortex methods*, Ph.D. thesis, University of California, Berkeley, CA, 1984.

[18] O. H. HALD AND V. M. DEL PRETE, *Convergence of vortex methods for Euler's equations*, Math. Comp., 32 (1978), pp. 791–809.

[19] O. H. HALD, *The convergence of vortex methods*, II, SIAM J. Numer. Anal., 16 (1979), pp. 726–755.

[20] O. H. HALD, *Convergence of a random method with creation of vorticity*, SIAM J. Sci. Statist. Comput., 7 (1986), pp. 1373–1386.
[21] ———, *Convergence of vortex methods for Euler's equations*, III, SIAM J. Numer. Anal., 24 (1987), pp. 538–582.
[22] J. M. HAMMERSLEY AND D. C. HANDSCOMB, *Monte Carlo Methods*, Methuen, London, 1964.
[23] L. D. LANDAU AND E. M. LIFSHITZ, *Fluid Mechanics*, Pergamon Press, New York, 1959.
[24] D. G. LONG, *Convergence of the random vortex method in one and two dimensions*, Ph.D. thesis, University of California, Berkeley, CA, 1986.
[25] E. G. PUCKETT, *Convergence of a random particle method to solutions of the Kolmogorov equation*, Math. Comp., 52 (1989), to appear.
[26] ———, *A study of the vortex sheet method and its rate of convergence*, Preprint 23341, Lawrence Berkeley Laboratory, University of California, Berkeley, CA, 1987.
[27] E. G. PUCKETT AND S. B. BADEN, *A fast vortex code for computing 2-d flow in a box*, Proc. First National Fluid Dynamics Congress, Cincinnati, OH, 1988.
[28] S. G. ROBERTS, *Accuracy of the random vortex method for a problem with non-smooth initial conditions*, J. Comput. Phys., 58 (1985), pp. 29–43.
[29] ———, *Convergence of a random walk method for Burgers' equation*, Ph.D. thesis, University of California, Berkeley, CA, 1985.
[30] H. SCHLICHTING, *Boundary-Layer Theory*, McGraw-Hill, New York, 1968.
[31] M. H. SCHULTZ, *Spline Analysis*, Prentice-Hall, Inc., Englewood Cliffs, NJ, 1973.
[32] J. A. SETHIAN AND A. F. GHONIEM, *Validation study of vortex methods*, J. Comput. Phys., 74 (1988), pp. 283–317.
[33] J. A. SETHIAN, *Turbulent combustion in open and closed vessels*, J. Comp. Phys., 55 (1984), pp. 425–456.
[34] ———, *Vortex Methods and Turbulent Combustion*, Lectures in Applied Mathematics 22, Springer-Verlag, New York, Berlin, 1985.
[35] D. M. SUMMERS, T. HANSON, AND C. B. WILSON, *A random vortex simulation of wind-flow over a building*, Internat. J. Numer. Methods Fluids, 5 (1985), pp. 849–871.
[36] E. TIEMROTH, *The simulation of the viscous flow around a cylinder by the random vortex method*, Ph.D. thesis, Naval Arch. Department, University of California, Berkeley, CA, 1986.
[37] F. M. WHITE, *Viscous Fluid Flow*, McGraw-Hill, New York, 1974.